ALL-OPTICAL MICROWAVE SIGNAL PROCESSING

By

Yichen Han

Thesis submitted to the

Faculty of Graduate and Postdoctoral Studies

In partial fulfillment of the requirements of

Master of Applied Science

Ottawa-Carleton Institute of Electrical and Computer Engineering

School of Electrical Engineering and Computer Science

University of Ottawa

ACKNOWLEDGEMENTS

First of all, I would like to express my great gratitude to my thesis advisor, Professor Jianping Yao, for providing me with excellent research environment, valuable directions and delicate guidance throughout this research work. His meticulous scholarship impresses me. His great passion towards scientific research work inspires me to work hard. His rich knowledge has made him as a constant source of ideas. Without his encouragement and patience, this work would have never been finished.

Special thanks to Ze Li, for his generosity in sharing his knowledge with me. Sincere thanks to his invaluable help in encouraging me to overcome obstacles in the research.

I would also like to thank the current and former colleagues in the Microwave Photonics Research Laboratory at the School of Information Technology and Engineering, University of Ottawa: Shilong Pan, Chao Wang, Ming Li, Wangzhe Li, Honglei Guo, Weilin Liu, Hiva Shahoei, Hongqian Mu and Junqiang Zhou. Their strong support and generous help greatly improved my research work. The memory of working with them is one of the most precious treasures in my life.

Finally I am greatly indebted to my beloved family: my father Qun Han, my mother Peijin Gong, all my aunts and my cousins. They have always been the biggest support, physically and mentally, to my life and study.

TABLE OF CONTENTS

LIST OF FIGURES

ABSTRACT

Microwave signal processing in the optical domain is investigated in this thesis. Two signal processors including an all-optical fractional Hilbert transformer and an all-optical microwave differentiator are investigated and experimentally demonstrated.

Specifically, the photonic-assisted fractional Hilbert transformer with tunable fractional order is implemented based on a temporal pulse shaping system. The fractional Hilbert transformer consists of a phase modulator and two dispersive elements with complementary dispersion. The fractional Hilbert transform is realized if a step function is applied to the phase modulator to introduce a phase jump. The proposed technique is investigated numerically and experimentally. The results show that a real-time fractional Hilbert transformer is achieved with a tunable fractional order by tuning the step function applied to the phase modulator.

The microwave bandpass differentiator is implemented based on a finite impulse response (FIR) photonic microwave delay-line filter with nonuniformly-spaced taps. To implement a microwave bandpass differentiator, the coefficients of the photonic microwave delay-line filter should have both positive and negative coefficients. In the proposed approach, the negative coefficients are equivalently achieved by introducing an additional time delay to each of the taps, leading to a π phase shift to the tap. Compared with a uniformly-spaced photonic microwave delay-line filter with true

negative coefficients, the proposed differentiator features a greatly simplified implementation. A microwave bandpass differentiator based on a six-tap nonuniformly-spaced photonic microwave delay-line filter is designed, simulated, and experimentally demonstrated. The reconfigurability of the microwave bandpass differentiator is experimentally investigated. The employment of the differentiator to perform differentiation of a bandpass microwave signal is also experimentally demonstrated.

CHAPTER 1 INTRODUCTION

1.1 Background review

Microwave photonics is an interdisciplinary field that investigates the interaction between microwave and optical signals [1]-[3] for applications such as radar, wireless communications, imaging and modern instrumentation. In the past decades, there has been an increasing effort in researching microwave photonics techniques for the generation, distribution, control and processing of microwave signals in the optical domain.

The all-optical processing of microwave signals is one of the most important topics and has been researched extensively [4]-[6]. The key advantages of an all-optical microwave signal processor include high speed, large bandwidth, low loss and immunity to electromagnetic interference (EMI). Numerous signal processing architectures have been proposed. In general, a photonic microwave signal processor consists of three key modules, an electrical-to-optical conversion (E/O) module, to convert a microwave signal from the electrical domain to the optical domain, a signal processing module, and an electrical-to-optical conversion (O/E) module, to convert the processed signal to the electrical domain, as shown in Fig. 1.1. The key module is the signal processing module. For linear signal processing, all functions can be modeled as a filtering operation, by changing the magnitude and/or phase of a

microwave signal in the optical domain. In this thesis, our discussion will be focused on the design of two all-optical signal processors to perform fractional Hilbert transform and microwave bandpass differentiation. Specifically, the fractional Hilbert transform is implemented based on temporal pulse shaping technique [7].

Fig. 1.1 Photonic microwave signal processor.

Optical pulse shaping was originally proposed for photonic microwave arbitrary waveform generation (AWG). Numerous techniques have been proposed to achieve optical pulse shaping in the past decade [8]. In general, photonic-assisted microwave waveform generation can be classified into three categories, 1) direct space-to-time (DST) pulse shaping [9]-[15], 2) spectral-shaping and wavelength-to-time (SS-WTT) mapping [17]-[25], and 3) temporal pulse shaping (TPS) [26]-[30]. These techniques can be implemented using free space optics where a spatial light modulator (SLM) is usually employed to perform temporal or spectral shaping. The key advantage of the pulse shaping technique using free space optics is its reconfigurability. The spatial pattern on the SLM can be updated in real time. The major limitation of a pulse shaping system based on free space optics is the large size. In addition, a strict alignment of the devices is needed which makes the system complicated. A solution to this problem is to perform pulse shaping based on fiber optics.

Pulse shaping for photonic-assisted microwave AWG has been demonstrated based on DST mapping [9]-[15]. In a DST system, the spectrum of an ultrashort (~femtosecond) input optical pulse is mapped to the spatial domain. The magnitude and the phase spectrum of the pulse can be directly manipulated by a DST pulse shaper. Through controlling the spatial pattern on the pulse shaper, arbitrary phase and amplitude modulation on the input pulse can be obtained. A DST pulse shaper can be either implemented using free space optics such as an SLM or fiber optics such as an arrayed waveguide gratings.

Pulse shaping for microwave AWG can also be implemented based SS-WTT. [16]-[23]. In a SS-WTT mapping system, an ultrashort pulse from a mode-locked laser source is sent to a spectral shaper. The spectral shaping (SS) is then achieved using an optical filter such as an SLM [16] or a fiber Bragg grating (FBG) [17]-[22]. The wavelength-to-time (WTT) mapping is realized in a dispersive element, such as a dispersive fiber or a linearly-chirped FBG (LC-FBG) [24] [25]. An arbitrary microwave waveform with its shape that is identical to the shaped spectrum is obtained at the output of a photodetector (PD). The key feature of this technique is that pulse shaping is implemented in the frequency domain. Therefore, an ultra-fast temporal waveform can be generated using a spectral shaper without the need of high-speed processing in the time domain.

Pulse shaping in the optical domain can also be achieved based on a TPS system. TPS has been extensively investigated in the past few years due to its important applications in areas such as frequency analysis [26] and AWG [27]-[30]. The concept of TPS was originally proposed by Heritage and Weiner [9] based on free space optics. In [26], a TPS system was employed for the analysis of the spectrum of a microwave signal. Since the output in the TPS system is in the time domain, a fast measurement of the spectrum could be implemented using a real-time oscilloscope. The most important application of the TPS technique is to achieve AWG [27]-[30]. Since the output waveform is determined by the modulation signal, the output waveform to be generated can be programmed in real time [27] [28]. In addition, the use of a TPS system incorporating a phase modulator can generate a pulse burst with tunable repetition rate [29]. Recently, a TPS system to generate a high frequency and frequency-chirped microwave waveform was demonstrated [30]. A typical TPS system consists of two dispersive elements (DEs) with complementary dispersion and an electro-optic modulator (EOM) between the two dispersive elements. A transform-limited ultrashort optical pulse is firstly stretched by the first DE, so that the dispersed pulse is temporally wide enough and can be modulated by a microwave modulation pattern applied to the EOM. The modulated signal is then compressed by the second DE. The key feature of the TPS system is that the generated waveform at the output of the system is the Fourier transform (FT) of the modulation microwave signal. Therefore, an ultra-fast microwave signal can be generated using a relatively low-speed modulation microwave signal.

The above three pulse shaping techniques for microwave AWG have been applied to the field of microwave signal processing. Photonic microwave signal processing via SLM-based pulse shaping technique have been demonstrated in [31]-[35]. Photonic microwave signal processors, such as temporal differentiator, integrator and Hilbert transformer, based on fiber-optics-based spectral shaping using FBGs were reported in [36]-[42]. A temporal differentiator can be achieved using a π-phase shift fiber Bragg grating (PS-FBG) [37], a long-period fiber grating [36] [38], or a special FBG designed using the discrete layer peeling (DLP) method [39]. The FBG using DLP method has also been employed to design an arbitrary-order temporal integrator [40]. A Hilbert transformer can also be implemented in the optical domain based on a PS-FBG [41], with a bandwidth as large as a few hundred of gigahertz, and a fractional Hilbert transformer based on a directly designed FBG using the DLP method was proposed in [42]. The use of a TPS system for photonic microwave signal processing has also been reported [43].

Other than realizing photonic microwave signal processing using pulse shaping techniques, discrete-time optical processing of microwave signals is also a widely used method for photonic microwave signal processing. Due to the limited speed of the currently available digital electronics, the processing of a high-frequency and broadband signal based on photonic techniques has been considered a promising solution. Among many signal processing schemes, the one based on a delay-line

architecture with a finite impulse response (FIR) has been widely investigated, which can find numerous applications such as spectral filtering, phase coding, and chirped microwave signal generation or chirped pulse compression. The first work of utilizing delay lines for signal processing can be tracked back to the article by Wilner and Van de Heuvel in 1976 [44]. In the past three decades, extensive efforts have been devoted to the exploration of photonic microwave filters [2] [4]-[6] [45].

In general, a microwave signal under processing is modulated on an optical carrier or an array of optical carriers, time delayed, added in the optical domain, and then converted back to the electrical domain using a PD. To avoid optical interference, a photonic microwave filter is usually operating in the incoherent regime. The major limitation of a microwave delay-line filter operating in the incoherent regime is the all-positive nature of the tap coefficients, which makes the FIR filter low-pass only. For many applications, however, a band-pass filter with negative or complex coefficients is needed. In order to overcome this problem, numerous techniques have been proposed to achieve an FIR filter with negative tap coefficients [46]-[57]. Photonic microwave delay-line filters with complex tap coefficients have also been proposed [58] [59]. A photonic microwave filter with complex coefficients can have an arbitrary spectral response, which is highly needed for advanced signal processing. Although the schemes in [58] [59] can provide complex coefficients, the implementation is extremely complicated, especially when the number of taps is large. To solve this problem, Dai and Yao recently developed a concept to design and

realize a bandpass microwave photonic filter with equivalent negative or complex tap coefficients [60] [61]. Instead of using a delay-line structure with uniformly spaced taps, the filter has a structure with nonuniformly spaced taps, or more precisely, each tap has an additional time delay, corresponding to an additional phase shift, making the coefficient of the specific tap have an equivalent negative or complex coefficient. Based on this concept, advanced signal processing functions, such as phase coding, chirped microwave signal generation and chirped pulse compression have been demonstrated [61].

In this thesis, our efforts are directed to the implementation of two photonic assisted signal processors to implement a fractional Hilbert transformer based on a TPS system and a bandpass microwave differentiator based on a nonuniformly spaced microwave photonic filter.

1.2 Major contribution of this thesis

One all-optical signal processors to achieve fractional Hilbert transform and another one to achieve microwave bandpass differentiation are proposed and experimentally demonstrated.

The fractional Hilbert transformer with a tunable fractional order is implemented based on TPS. The fractional Hilbert transformer consists of a phase modulator and two dispersive elements with complementary dispersion. The fractional Hilbert

transform is realized if a step function is applied to the phase modulator to introduce a phase jump. The proposed technique is investigated numerically and experimentally. The results show that a real-time Hilbert transform is achieved with a tunable fractional order by tuning the step function applied to the phase modulator.

The microwave bandpass differentiator is implemented based on a FIR photonic microwave delay-line filter with nonuniformly-spaced taps. To implement a microwave bandpass differentiator, the coefficients of the photonic microwave delay-line filter should have both positive and negative coefficients. In the proposed approach, the negative coefficients are equivalently achieved by introducing an additional time delay to each of the taps, leading to a π phase shift to the tap. Compared with a uniformly-spaced photonic microwave delay-line filter with true negative coefficients, the proposed differentiator features a greatly simplified implementation. A microwave bandpass differentiator based on a six-tap nonuniformly-spaced photonic microwave delay-line filter is designed, simulated, and experimentally demonstrated. The reconfigurability of the microwave bandpass differentiator is experimentally investigated. The employment of the differentiator to perform differentiation of a bandpass microwave signal is also experimentally demonstrated.

1.3 Organization of this thesis

The thesis consists of six chapters. In Chapter 1, a brief background review of microwave signal processing using photonics is presented. Then, the major contributions of this thesis are summarized.

In Chapter 2, the theoretical background of temporal pulse shaping is reviewed. The implementation of a temporal pulse shaping system based on free space optics is reviewed. Then the operation of a temporal pulse shaping system using fiber optics is introduced.

In Chapter 3, photonic microwave signal processing based on a microwave photonic delay-line filter is reviewed. The operation of a microwave photonic delay-line filter is firstly presented. Then, the techniques to implement a photonic microwave filter with true negative and complex tap coefficients are introduced. Finally, the implementation of a photonic microwave delay-line filter with nonuniformly spaced taps to achieve an arbitrary spectral response is discussed.

In Chapter 4, a photonic-assisted fractional Hilbert transformer with tunable fractional order implemented based on a TPS system is proposed and experimentally demonstrated. The fractional Hilbert transformer consists of a phase modulator and two dispersive elements with complementary dispersion. The fractional Hilbert transform is realized if a step function is applied to the phase modulator to introduce a

phase jump. The performance of the fractional Hilbert transformer is evaluated based on simulations and experiments.

In Chapter 5, a photonic microwave bandpass temporal differentiator implemented based on a photonic microwave delay-line filter with nonuniformly-spaced taps is proposed and experimentally demonstrated. The bandpass differentiator is implemented based on a FIR photonic microwave delay-line filter with nonuniformly-spaced taps. To implement a microwave bandpass differentiator, the photonic microwave delay-line filter should have both positive and negative coefficients. In the proposed approach, the negative coefficients are equivalently achieved by introducing an additional time delay to each of the taps, leading to a π phase shift to the tap. Compared with a uniformly-spaced photonic microwave delay-line filter with true negative coefficients, the proposed differentiator features a greatly simplified implementation. The performance of the differentiator is evaluated based on simulations and experiments.

In Chapter 6, a conclusion is drawn and the future work for this research is discussed.

CHAPTER 2 TEMPORAL PULSE SHAPING TECHNIQUES – A REVIEW

2.1 Theoretical background of temporal pulse shaping techniques

The objective of pulse shaping is to shape an ultrashort optical pulse either in the temporal or in the frequency domain to generate a waveform with the desired temporal or spectral attributes, which can find numerous applications such as in optical communications, radar, wireless communications, femtochemistry, warfare systems, and medical imaging systems. For example, pulse shaping has been used to generate monocycle and doublet pulses for ultra-wide band (UWB) communications [17].

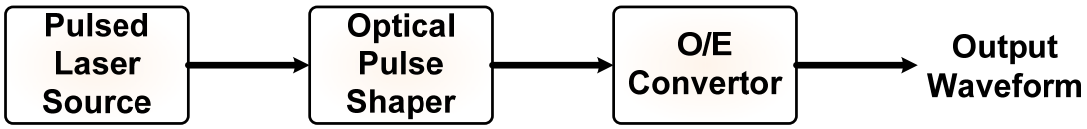

Fig. 2.1 Schematic of a pulse shaping system.

As shown in Fig. 2.1, a pulse shaping system consists of a pulsed laser source, an optical pulse shaping filter and an O/E converter. An ultrashort transform-limited pulse with a temporal duration in the order of femtoseconds is generated using a pulsed laser source, such as an actively or passively mode-locked laser (MLL). For example, the experiment in this thesis for the fractional Hilbert transform is performed using a passively MLL that can generate an ultrashort optical pulse with a

temporal width of 550 fs and a 3-dB bandwidth of 8 nm. Then, the ultrashort pulse is shaped by an optical pulse shaper either in free space optics or fiber optics. Finally, the shaped waveform is converted from the optical domain to the electrical domain using an O/E convertor which is usually a PD. At the output of the system, a microwave waveform with the desired temporal or spectral attributes is generated. As discussed in Chapter 1, photonic-assisted microwave waveform generation can be classified into three categories, 1) direct space-to-time (DST) pulse shaping, 2) spectral-shaping and wavelength-to-time (SS-WTT) mapping, 3) temporal pulse shaping (TPS). Since the fractional Hilbert transform reported in this thesis is achieved based on the TPS technique, only the TPS technique implemented using either free space optics or fiber optics is reviewed in this chapter.

A temporal pulse shaping system can be modeled as a linear, time-invariant (LTI) system. A LTI system can be characterized using the system impulse response $h(t)$. As shown in Fig. 2.2, for an input signal $x(t)$, the temporal waveform at the output of the LTI system equals to the convolution between input signal $x(t)$ and system impulse response $h(t)$

$$y(t) = x(t) * h(t) \tag{2-1}$$

where $y(t)$ is the temporal signal at the output of the LTI system, and * denotes the convolution operation.

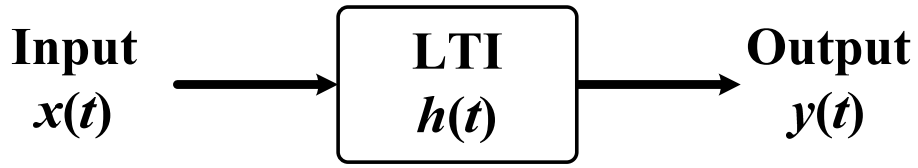

Fig. 2.2 An LTI system with an impulse response $h(t)$.

In the frequency domain, the LTI system can be characterized using a system transfer function $H(\omega)$, which is the FT of the temporal impulse response. As shown in Fig. 2.3, the convolution in the time domain becomes multiplication in the frequency domain. The output signal in the frequency domain is thus given

$$Y(\omega) = X(\omega) \cdot H(\omega) \tag{2-2}$$

where $X(\omega)$, $Y(\omega)$ and $H(\omega)$ are the Fourier transforms of $x(t)$, $y(t)$ and $h(t)$.

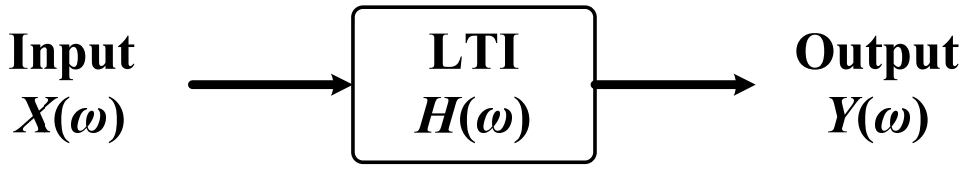

Fig. 2.3 An LTI system characterized by a transfer function $H(\omega)$.

If the input signal is a Dirac delta function, the output waveform is thus identical to impulse response $h(t)$. In a pulse shaping system, an ultrashort input pulse is used as an input, which can be considered as a Dirac delta function, thus the generation of a

desirable waveform reduce to a problem to design the system impulse response $h(t)$, or equivalently, the frequency response $H(\omega)$.

2.2 Temporal pulse shaping based on free space optics

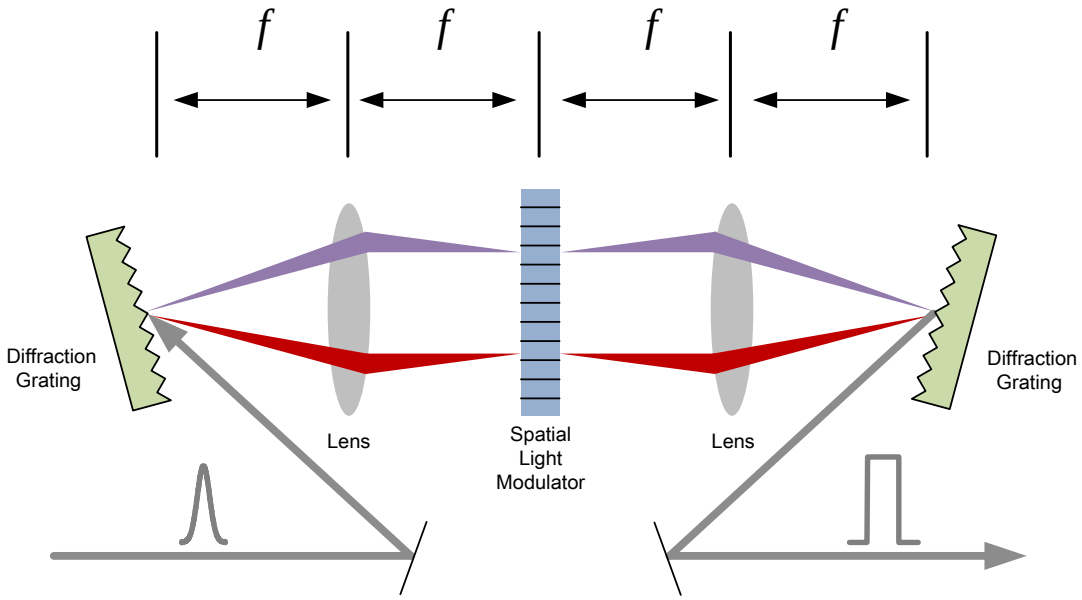

Fig. 2.4 System configuration of a TPS system based on free space optics.

A TPS system based on free space optics is shown in Fig. 2.4. The system consists of a pair of diffraction gratings, a pair of lenses, and a SLM. The SLM here is a spatial mask with a spatially patterned amplitude and phase mask. The distance between the left grating and the left lens, the left lens and the SLM, the SLM and the right lens, the right lens and the right grating is the focal length of the lens. Thus, the system is also referred to as a "4-f" pulse shaping system. An ultrashort optical pulse is sent to the left grating which is dispersed by the grating. Then, the angularly dispersed signal is

focused to spots along one dimension at the back focal plane of the left lens. The left diffraction grating and the lens perform a FT of the input signal. The FT of the incident pulse is achieved as a spatial separation at the back focal plane of the left lens. An SLM with a spatially patterned amplitude mask, as shown in Fig. 2.5(a), and a spatially patterned phase mask, as shown in Fig. 2.5(b), is placed in the plane in order to manipulate the FT of the input signal. Then, the filtered spatial pattern is recombined into a single collimated beam by the right lens and the diffraction grating. The right lens and the diffraction grating perform inversed FT to the shaped pattern. The signal with a waveform approximately identical to the FT of the spatially distributed pattern is obtained at the output of the system. For example, if we impose a sinc function pattern on the SLM, a signal with a temporal waveform of a rectangular impulse would be obtained at the output of the system.

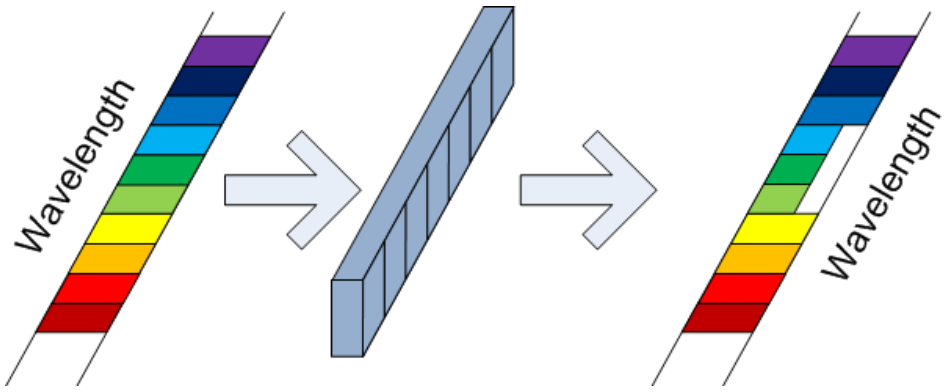

Fig. 2.5 (a) A spatially patterned amplitude mask.

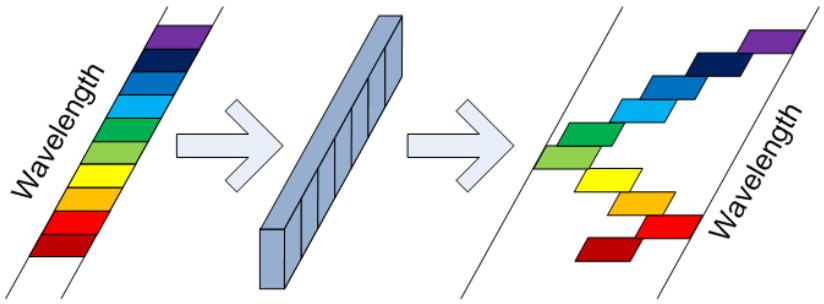

Fig. 2.5 (b) A spatially patterned phase mask.

As shown in Fig. 2.5(a), a magnitude function can be imposed onto the spectrum of the incident signal by controlling the transmission rate of different spots on the amplitude mask. Similarly, a phase function can be imposed onto the spectrum of the input pulse through adjusting the refraction index of different area on the mask. After processed by the phase only mask, the magnitude of the spectrum under processing stays the same but the phase response is updated. Through the co-effect of the amplitude and phase mask, an arbitrary spatially distributed pattern can be written on the SLM. Thus, an arbitrary waveform can be generated at the output of this system.

A SLM realized using fixed spatial mask was initially adopted in the early experiments and it was shown to have excellent quality in temporal pulse shaping. However, the fixed pattern leads to the poor programmability. Once the mask is fabricated, the spatially distributed pattern on the mask is fixed. A fixed spatial mask can only be used to generate a single waveform. If we want to generate a different waveform at the output of the system, a new mask is needed. For many applications,

an arbitrary waveform is needed, thus an optical pulse shaper should be updated in real time. A solution is to use a programmable SLM. In the following, a programmable SLM realized using a liquid crystal-SLM (LC-SLM) and an Acousto-optic modulator (AOM) will be discussed.

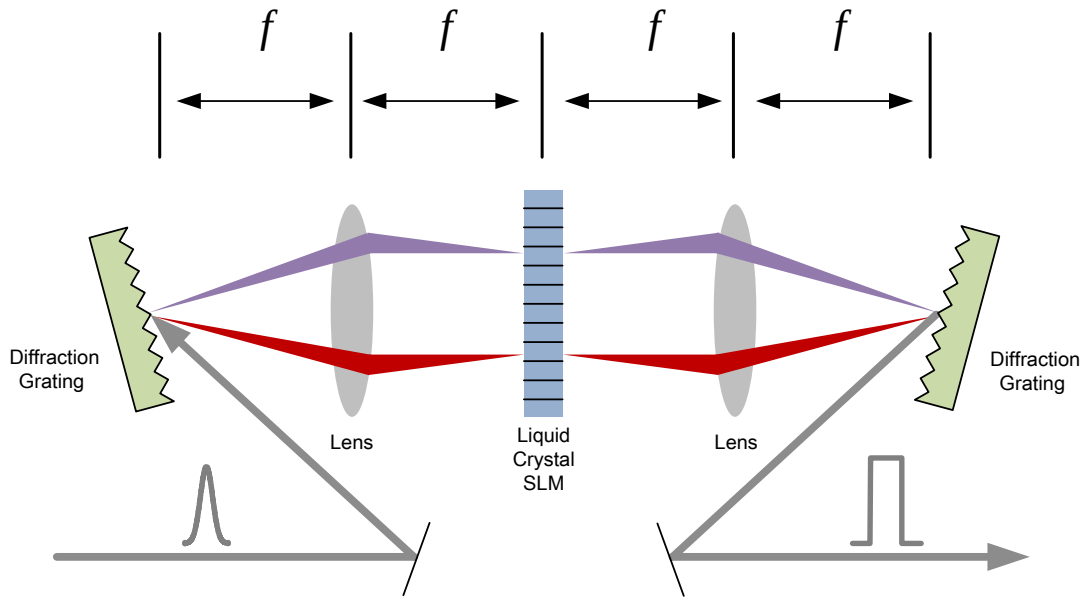

Fig. 2.6 Schematic of a pulse shaping system based on an LC-SLM.

The system configuration of a pulse shaping system using an LC-SLM is shown in Fig. 2.6. The fixed spatial mask is replaced by an LC-SLM. An LC-SLM consists of a pair of half-wave plates and a liquid crystal modulator array. The plates are used to rotate the polarization of the incident light in order to satisfy the input requirement of liquid crystal modulator array. The front view of the liquid crystal array is shown in Fig. 2.7. The rectangular shapes are pixels and the gap between adjacent pixels is called dead space. By addressing the controlling electrical signal, a spatially spectral waveform pattern is generated on the modulator plane.

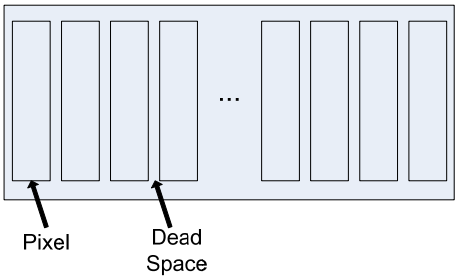

Fig. 2.7 Front view of an LC-SLM.

An AOM is another programmable SLM. The system configuration of a pulse shaper based on an AOM is given in Fig. 2.8. The programmable SLM is now an AOM. The AOM is fabricated on an AOM crystal which is usually TeO_2 or InP.

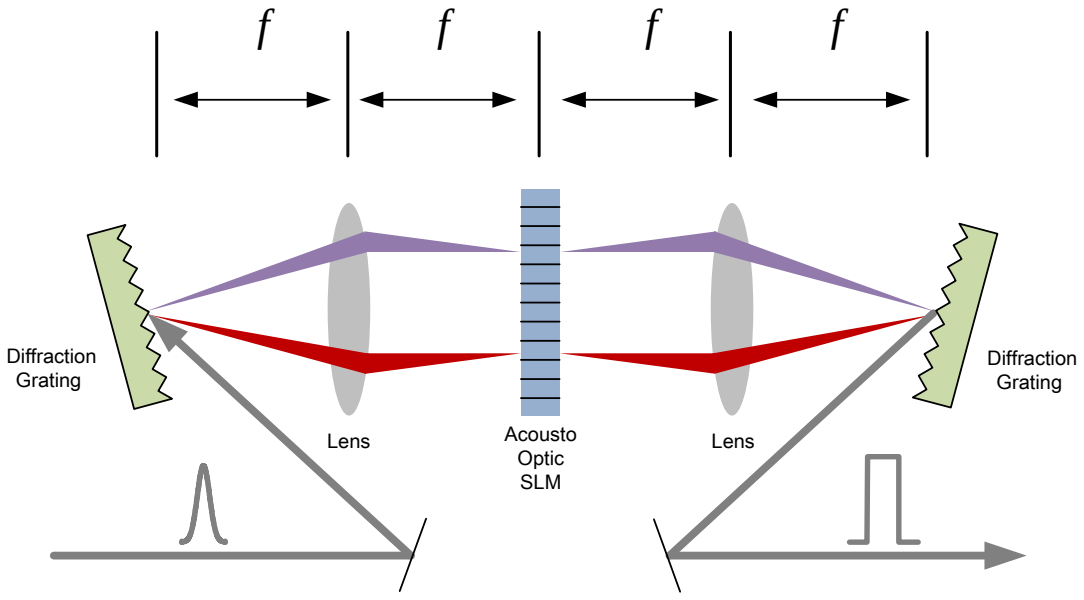

Fig. 2.8 Schematic of a pulse shaping system based on an AOM.

The structure of an AOM is shown in Fig. 2.9. An AOM consists of a piezoelectric transducer and an AOM crystal. The AOM is driven by a radio frequency (RF) signal

generator. A RF driving signal is loaded on the piezoelectric transducer, the black rectangular block in the diagram, and is converted into a traveling acoustic wave. The acoustic wave goes through the AOM crystal, generating a grating with a periodically changed refractive index along the crystal. The transfer function of the spatial grating generated inside the AOM crystal is determined by the driving signal applied to the transducer, and hence the spatial pattern generated on the modulator is determined.

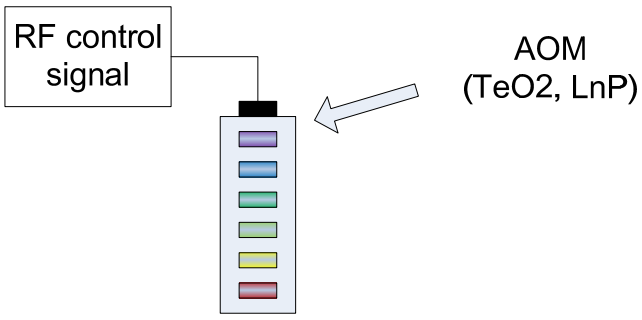

Fig. 2.9 Structure of an AOM.

2.3 Temporal pulse shaping technique based on fiber based optics

The key advantage of a temporal pulse shaping system using free space optics is its programmability. The spatial pattern on the SLM can be updated at a high rate. The major limitation of a temporal pulse system based on free space optics is the large size. In addition, the need for strict and precise alignment of the devices makes the system complicated and costly. Furthermore, the coupling between free-space to fiber and fiber to free-space makes the system very lossy. A solution to these problems is to use fiber optics.

Before we discuss fiber-optic TPS techniques, we give a short review of real-time Fourier transform based on a dispersive fiber-optic element. Similar to a diffraction grating for which the diffracted pattern is a Fourier transformed version of the incident light pattern in the spatial domain, which is employed in free-space TPS systems, as illustrated in Fig. 2.4. A similar conclusion is drawn for a fiber-optic dispersive element, in the temporal domain. If a transform-limited ultrashort optical pulse passes through a dispersive element such as a length of SMF or a LC-FBG, the signal at the output of the dispersive element is a Fourier transformed version of the input signal [24] [25]. Therefore, the dispersive element performs a real-time FT to the incident optical pulse. Since the output temporal waveform has a shape that is a scaled version of the spectrum of the incident signal, this operation is also known as frequency-to-time (FTT) mapping or wavelength-to-time (WTT) mapping. A temporal pulse shaping system based on fiber-optics is established based on this concept.

The concept of the frequency to time conversion is shown in Fig. 2.10. In the time domain, the dispersive element, such as a length of SMF or a LC-FBG, can be characterized as an LTI system with a temporal impulse response given by [25]

$$h_{\ddot{\Phi}}(t) = C \exp\left(-\frac{j\pi t^2}{\ddot{\Phi}} \right) \tag{2-3}$$

where C is a constant and $\ddot{\Phi}$ is the group velocity dispersion of the dispersive medium.

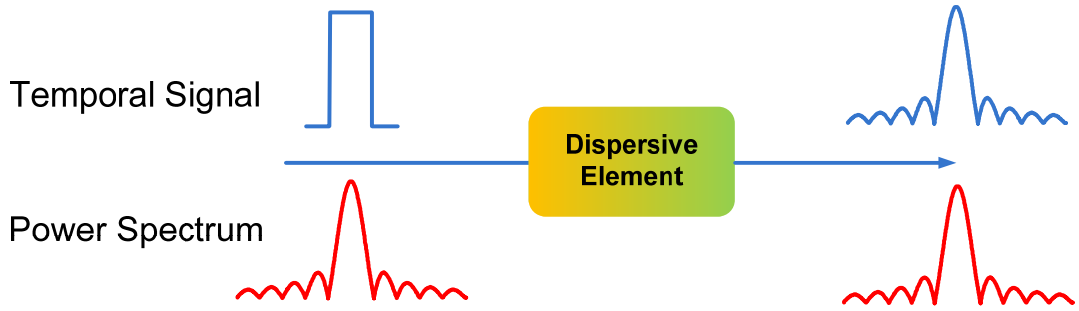

Fig. 2.10 Frequency-to-time mapping in a dispersive element.

If a transform-limited optical pulse with a complex waveform $x(t)$ goes through this dispersive medium, the output complex waveform $y(t)$ can be calculated by the convolution of the input waveform and the impulse response of the dispersive element $h_{\ddot{\Phi}}(t)$

$$\begin{aligned} y(t) = x(t) * h_{\ddot{\Phi}}(t) &= C\int_{-\infty}^{+\infty} x(\tau)\exp\left[-\frac{j\pi(t-\tau)^2}{\ddot{\Phi}}\right]d\tau \\ &= C\exp\left(-\frac{j\pi t^2}{\ddot{\Phi}}\right)\int_{-\infty}^{+\infty} x(\tau)\exp\left(-\frac{j\pi\tau^2}{\ddot{\Phi}}\right)\exp\left(\frac{j2\pi t\tau}{\ddot{\Phi}}\right)d\tau \end{aligned} \tag{2-4}$$

If the temporal width of $x(t)$ is sufficiently small and the dispersion of the dispersive element is large enough such that

$$\left|\frac{\Delta t^2}{\ddot{\Phi}}\right| << 1 \tag{2-5}$$

where Δt is the temporal width of the input pulse $x(t)$. Eq. (2-4) can be approximated by

$$\begin{aligned} y(t) &= C\exp\left(-\frac{j\pi t^2}{\ddot{\Phi}}\right)\int_{-\infty}^{+\infty} x(\tau)\exp\left(-\frac{j\pi\tau^2}{\ddot{\Phi}}\right)\exp\left(\frac{j2\pi t\tau}{\ddot{\Phi}}\right)d\tau \\ &= C\exp\left(-\frac{j\pi t^2}{\ddot{\Phi}}\right)\int_{-\infty}^{+\infty} x(\tau)\exp\left(\frac{j2\pi t\tau}{\ddot{\Phi}}\right)d\tau \\ &\approx C\exp\left(-\frac{j\pi t^2}{\ddot{\Phi}}\right)X(\omega)\Big|_{\omega=-\frac{2\pi t}{\ddot{\Phi}}} \end{aligned} \tag{2-6}$$

where $X(\omega)=\Im[x(t)]$ is the FT of the input temporal pulse $x(t)$. Obviously, the optical signal at the output of the dispersive element has a temporal envelope that is linearly proportional to the spectrum of the incident optical pulse with a phase factor.

The concept of FTT mapping is usually performed in the coherent regime. All the work done related to this concept within this thesis is using the FTT in the coherent regime. However, the FTT mapping can also be achieved using incoherent optical source such as an amplified spontaneous emission (ASE) source. Recently, incoherent FTT mapping has been reported to achieve incoherent pulse shaping [62] [63]. The incoherent pulse shaping technique has also been demonstrated to realize microwave signal processors [64] [65], such as a microwave signal integrator and correlator.

The concept of FTT mapping is employed in a fiber-optic TPS system. A typical TPS system consists of two dispersive elements with complementary dispersion and an electro-optic modulator (EOM). A transform-limited ultrashort optical pulse is first stretched by the first dispersive element so that the dispersed signal is temporally wide enough and can be modulated by a microwave modulation pattern applied to the EOM. Then the modulated signal is compressed by the second DE. The key feature of TPS system is that the generated waveform at the output of the system is the Fourier transform of the modulation microwave signal. Therefore, based on the Fourier transform property, a fast microwave waveform can be generated using a relatively low-speed modulation microwave signal.

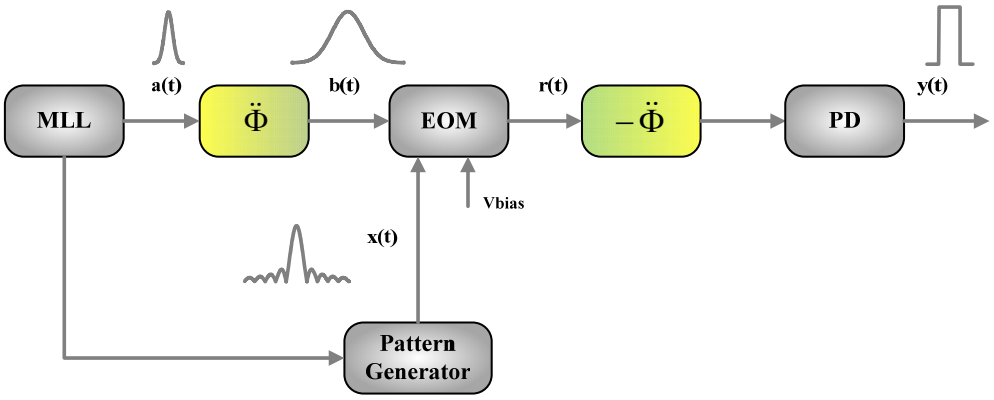

Fig. 2.11 System configuration of a temporal pulse shaping system.

Mathematically, the two DEs with complementary dispersion can be characterized using impulse response functions given by

$$h_{\ddot{\Phi}}(t) = C_1 \exp\left(-\frac{j\pi t^2}{\ddot{\Phi}}\right) \tag{2-7a}$$

and

$$h_{-\ddot{\Phi}}(t) = C_2 \exp\left(\frac{j\pi t^2}{\ddot{\Phi}}\right) \tag{2-7a}$$

where $\ddot{\Phi}$ is the group velocity dispersion, C_1 and C_2 are two constants.

Let $a(t)$ and $b(t)$ be the complex envelops of the signals at the input and the output of the first DE, respectively. Then, if the temporal width of $a(t)$ is sufficiently small and the dispersion of the dispersive element is large enough to satisfy the condition in (2-5), the output waveform of the first $b(t)$ can be approximated by

$$b(t) \approx C_1 \exp\left(-\frac{j\pi t^2}{\ddot{\Phi}}\right) A(\omega)\Big|_{\omega=-\frac{2\pi t}{\ddot{\Phi}}} \tag{2-8}$$

where $A(\omega) = \Im[a(t)]$ is the FT of the input temporal pulse $a(t)$. This process can be simply understood as the concept of FTT mapping in a dispersive element, as it was discussed earlier in this subsection. The first DE performs as a real-time Fourier transform of the input signal.

If the EOM is a phase modulator (PM) and a microwave modulation signal function $x(t)$ is applied to the EOM, the phase-modulated signal at the output of the EOM is given by

$$\begin{aligned} r(t) &= b(t)\cdot\exp\left(j\pi\frac{x(t)}{V_\pi}\right) \\ &= C_1\exp\left(-\frac{j\pi t^2}{\ddot{\Phi}}\right)\left\{A(\omega)\exp\left[j\varphi(\omega)\right]\right\}\Big|_{\omega=-\frac{2\pi t}{\ddot{\Phi}}} \end{aligned} \tag{2-9}$$

where V_π is the half-wave voltage of the PM and

$$\varphi(\omega)\big|_{\omega=-\frac{2\pi t}{\ddot{\Phi}}} = \pi\frac{x(t)}{V_\pi} \tag{2-10}$$

The modulated signal is then sent to the second DE. At the output of the second DE, we have

$$\begin{aligned} y(t) &= r(t) * h_{-\ddot{\Phi}}(t) \\ &= C_1C_2\int_{-\infty}^{+\infty}\exp\left(-\frac{j\pi\tau^2}{\ddot{\Phi}}\right)\left\{\Im\left[a(t)\right]\times\exp\left[j\varphi(\omega)\right]\right\}\Big|_{\omega=-\frac{2\pi\tau}{\ddot{\Phi}}}\times\exp\left[\frac{j\pi(t-\tau)^2}{\ddot{\Phi}}\right]d\tau \\ &= C_1C_2\,\ddot{\Phi}\exp\left(\frac{j\pi t^2}{\ddot{\Phi}}\right)\Im^{-1}\left\{A(\omega)\cdot\exp\left[j\varphi(\omega)\right]\right\}\Big|_{\omega=-\frac{2\pi t}{\ddot{\Phi}}} \end{aligned} \tag{2-11}$$

where $\Im^{-1}$ denotes the inverse FT operation. From (2-11), we may easily find out that a phase response $j\varphi(\omega)\big|_{\omega=-\frac{2\pi t}{\ddot{\Phi}}} = j\pi\frac{x(t)}{V_\pi}$ can be imposed onto the spectrum of the input ultrashort optical pulse. The phase response is proportional to the modulation signal $x(t)$.

Assume that the EOM is an intensity modulator (IM), and the IM is biased at the minimum transmission point. If a microwave modulation signal function $x(t)$ is applied to the IM, the modulated signal at the output of the IM is given by

$$\begin{aligned} r(t) &= b(t)\cdot\pi\frac{x(t)}{V_\pi} \\ &= C_1\exp\left(-\frac{j\pi t^2}{\ddot{\Phi}}\right)\left\{A(\omega)m(\omega)\right\}\Big|_{\omega=-\frac{2\pi t}{\ddot{\Phi}}} \end{aligned} \tag{2-12}$$

where V_π is the half-wave voltage of the IM and

$$m(\omega)\big|_{\omega=-\frac{2\pi t}{\ddot{\Phi}}} = \pi\frac{x(t)}{V_\pi} \tag{2-13}$$

The modulated signal is then sent to the second DE. At the output of the second DE, we have

$$
\begin{aligned}
y(t) &= r(t) * h_{-\ddot{\Phi}}(t) \\
&= C_1 C_2 \int_{-\infty}^{+\infty} \exp\left(-\frac{j\pi\tau^2}{\ddot{\Phi}}\right) \left\{ \Im\left[a(t)\right] \times m(\omega) \right\}\Big|_{\omega=-\frac{2\pi\tau}{\ddot{\Phi}}} \times \exp\left[\frac{j\pi(t-\tau)^2}{\ddot{\Phi}}\right] d\tau \\
&= C_1 C_2 \ddot{\Phi} \exp\left(\frac{j\pi t^2}{\ddot{\Phi}}\right) \Im^{-1}\left\{ A(\omega) \cdot m(\omega) \right\}\Big|_{\omega=-\frac{2\pi t}{\ddot{\Phi}}}
\end{aligned}
$$

(2-14)

From (2-14), we may easily find out that a magnitude response $m(\omega)\big|_{\omega=-\frac{2\pi t}{\ddot{\Phi}}} = \pi \frac{x(t)}{V_\pi}$ can be imposed onto the spectrum of the input ultrashort optical pulse. The magnitude response is proportional to the modulation signal $x(t)$.

Based on the theoretical analysis in the previous discussion, an arbitrary phase and magnitude response can be imposed to the input ultrashort optical pulse employing a PM and an IM, respectively. Thus, an arbitrary frequency and phase response can be achieved using a PM and an IM simultaneously.

2.4 Summary

In this chapter, the theoretical background of temporal pulse shaping was reviewed. The implementation of a temporal pulse shaping system based on free space optics and fiber optics was introduced. The objective of pulse shaping was to shape an ultrashort optical pulse either in the temporal or in the frequency domain to generate a waveform with the desired temporal or spectral attributes. A TPS system could be achieved using free space optics such as a “4-f” pulse shaping system, which could be configured in real-time by employing a LC-SLM or an AOM. The major limitation of

a pulse shaping system based on free space optics was the large size. In addition, a strict alignment of the devices was needed which makes the system complicated. Otherwise the system suffers from high coupling loss at the interface between the optics and the free space. A solution to this problem was to perform a TPS system based on fiber optics. In this chapter, a TPS system implemented using fiber optics was then modeled and theoretically analyzed.

CHAPTER 3 DISCRETE-TIME OPTICAL PROCESSING OF MICROWAVE SIGNALS – A REVIEW

In this chapter, we will first review the general concept of a delay-line transversal filter. Then, the typical system structure and the operation principle of a photonic microwave delay-line transversal filter are introduced. Different methods to realize a photonic microwave filter with true negative and complex coefficients are summarized. Finally the concept of using a photonic microwave filter with nonuniformly spaced taps to generate equivalent negative and complex coefficients is presented.

3.1 Operation principle of a delay-line transversal filter

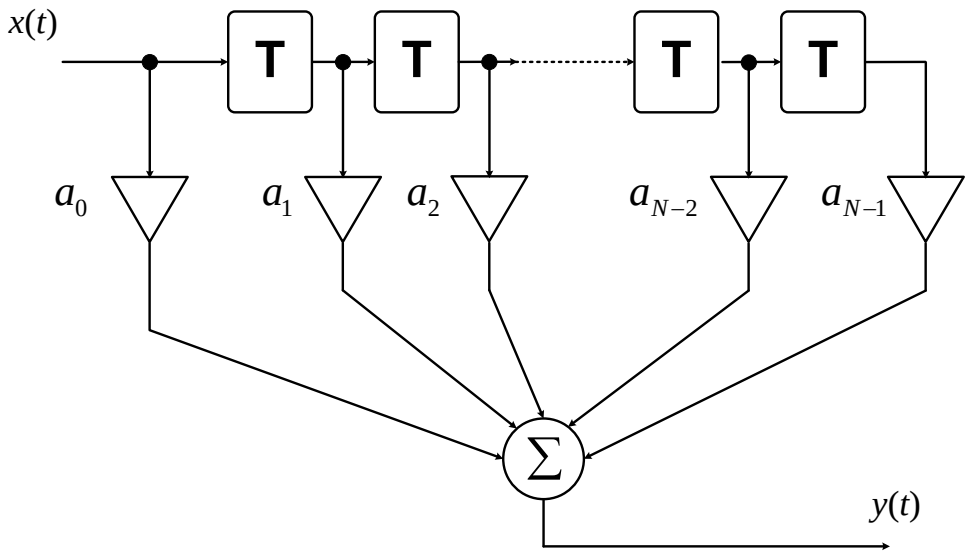

Fig. 3.1 Structure of a regular FIR filter with *N* uniformly spaced taps.

Since a photonic microwave filter with a non-recursive or FIR structure is easy to implement, which will be employed in this thesis for microwave signal processing, our discussion here will be focused on photonic microwave filters with a FIR structure. Fig. 3.1 shows the structure of a regular FIR filter with *N* uniformly spaced taps. As shown in Fig. 3.1, a FIR filter with *N* uniformly spaced taps consists of *N*-1 adders, *N*-1 unit delay elements and *N* constant multiplier. If the input signal is $x(t)$, the output signal $y(t)$ is given by

$$y(t)=\sum_{k=0}^{N-1}a_k x(t-kT) \tag{3-1}$$

where *N* is the number of the filter taps, a_k is the coefficient of the *k*-th tap and T is the time delay induced by a single unit delay elements. The free spectral range (FSR) of the FIR filter is given by

$$\Omega=\frac{2\pi}{T} \tag{3-2}$$

A FIR filter has a spectral response with multiple channels and any two adjacent channels are separated by an FSR of the filter. The center frequency of the *m*-th channel of the filter is $m\Omega$.

The system transfer function (or frequency response) of the regular FIR filter with uniformly spaced taps based on (3-1) can be calculated through FT by

$$H(\omega) = \sum_{k=0}^{N-1} a_k \exp\left(-jk\frac{2\pi}{\Omega}\omega\right) \tag{3-3}$$

As can be seen from (3-3), the frequency response of the FIR filter is determined by the number of the filter taps, the tap coefficients and the time spacing between adjacent taps.

3.2 Photonic microwave delay-line transversal filter

Due to the limited speed of the currently available digital electronics, the processing of high-frequency and broadband signal based on photonic techniques has been considered a promising solution. The advantages of a photonic microwave filter include large bandwidth, high speed, low loss, light weight and large tunability.

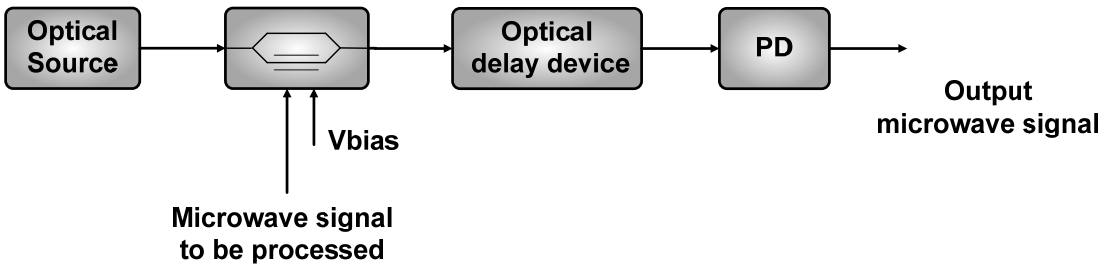

Fig. 3.2 Structure of a photonic microwave delay-line filter.

The structure of a photonic microwave delay-line filter is shown in Fig. 3.2. A photonic microwave filter consists of an optical source, an EOM, an optical time delay device, and a PD. The optical source could be a laser source, a laser array or an

ASE source. The microwave signal to be processed is modulated on one or multiple optical carriers using either an electro-optic phase modulator or an electro-optic intensity modulator. The modulated optical signal then goes through an optical time-delay device. A photonic microwave filter implemented using a single laser source and an array of optical delay lines is shown in Fig. 3.3 and a laser array and a single optical delay time shown in Fig. 3.4.

The diagram of a microwave filter using a single laser and an array of optical time delay lines with a FIR structure is shown in Fig. 3.3. It consists of a $1\times N$ splitting device, a modulator, N optical time delay components, an $N\times 1$ coupling device, and a PD. The splitting device can be an optical splitter and the time delay components can be fiber lines.

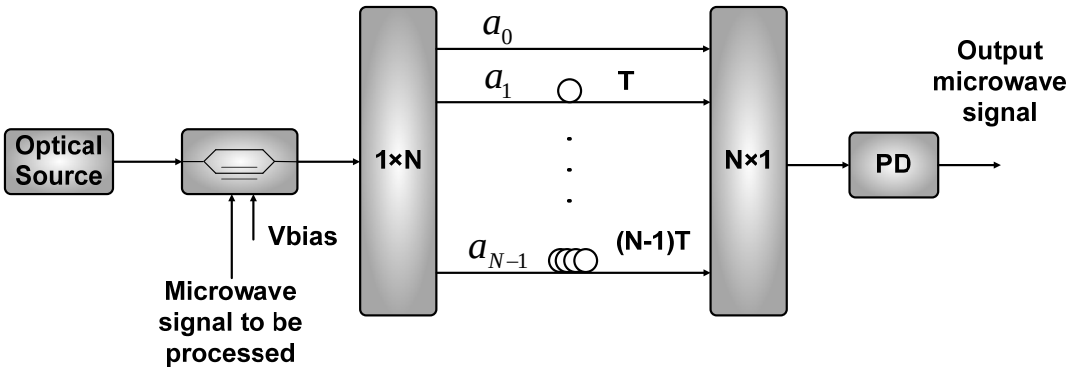

Fig. 3.3 Structure of a photonic microwave filter using a single laser source and an array of optical delay lines.

The modulated optical signal is split into multiple channels and the delayed with different time delays kT and multiplication coefficient a_k. The time delay between

adjacent channels is the unit time delay T. Then the signals from the channels are combined using an optical coupling device and sent to the PD. The filtered microwave signal is achieved at the output of the PD.

The diagram of a microwave filter using a laser array and a single optical time delay line is shown in Fig. 3.4. It consists of an $N \times 1$ combining device, an optical time delay component and a PD. The optical time delay component can be a length of dispersive fiber or a LCFBG.

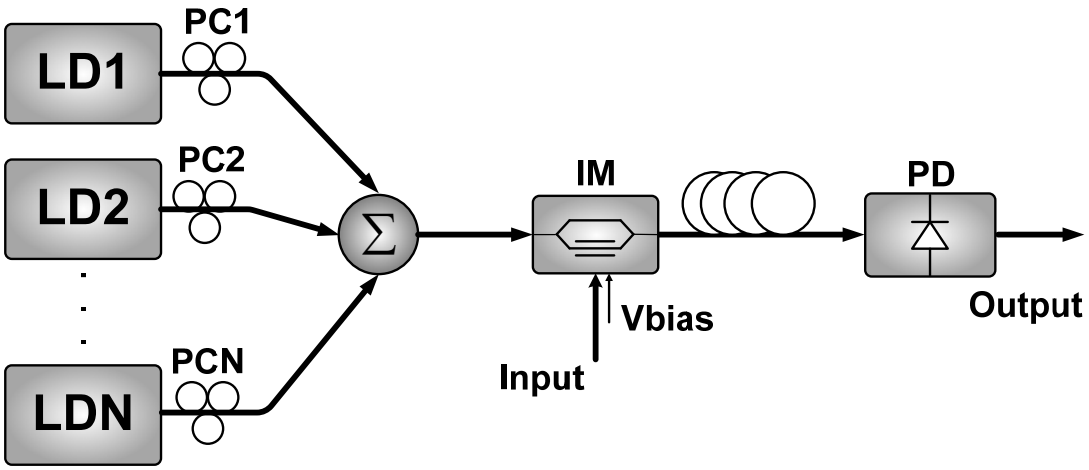

Fig. 3.4 System configuration of an *N*-tap photonic microwave filter using a laser array and a single delay line device.

The outputs from the laser array are combined using an *N*×1optical coupling device and modulated by a microwave signal to be processed. The optical source can be either an array of independent laser diodes or a sliced broadband source. Each optical wavelength generates a filter tap that is delayed by the dispersive element such as a

length of SMF, a LCFBG or a length of DCF. The dispersion of the dispersive element is chosen such that the differential group delay for the adjacent wavelengths of the optical array is T. The time delay between adjacent taps is given by

$$T = \frac{\Delta\lambda}{D \cdot L} \tag{3-4}$$

where $\Delta\lambda$ is the wavelength spacing between adjacent wavelengths, D is the dispersion parameter of the dispersive element (in ps/nm/km) and L is the length of the dispersive fiber.

The coherence time of an optical source is given by

$$\tau_{co} = \frac{1}{\pi \cdot \Delta\nu} \tag{3-5}$$

where $\Delta\nu$ is the source linewidth. If

$$\tau_{co} \gg T \tag{3-6}$$

is satisfied, the filter works in the coherent regime. It is possible for a photonic microwave filter to achieve negative tap coefficients in the coherent regime. However, the frequency response of the filter depends closely on the optical phase of the optical source which is sensitive to the environmental conditions. Most of the reported

photonic microwave filters are designed to work in the incoherent regime. In this case, only optical intensities are detected by the PD. Thus, a photonic microwave filter working in the incoherent regime has only positive tap coefficients. Based on signal processing theory, a delay-line filter with all positive tap coefficients will have a spectral response at the baseband, making the filter a low-pass only. For many applications, however, a band-pass filter with negative or complex coefficients is needed. Numerous techniques have been proposed to achieve a FIR bandpass filter by generating negative and complex tap coefficients in the incoherent regime.

3.3 Photonic microwave filter with true negative and complex tap coefficients

A straightforward way to implement a photonic microwave filter with true negative taps in the incoherent regime is to use differential photo detection [46]. As shown in Fig. 3.5, the system consists of an optical source, an electro-optic intensity modulator, an optical coupler and a balanced PD. The positive and negative tap coefficients are achieved by balanced detection in the electrical domain.

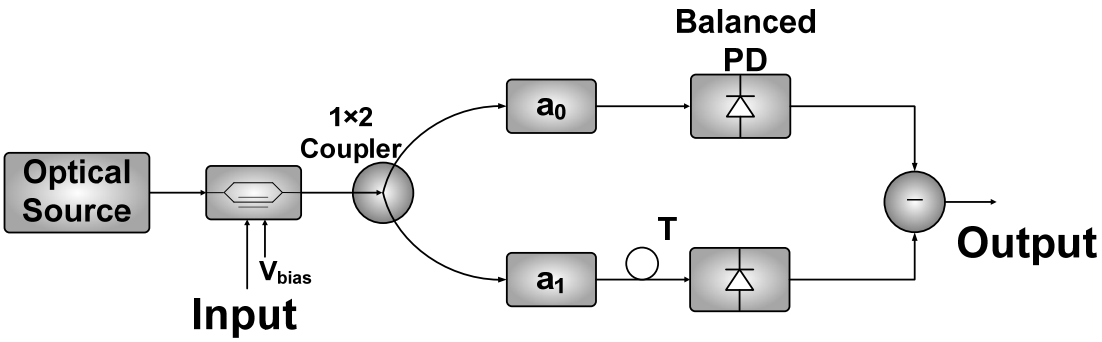

Fig. 3.5 System configuration of a photonic microwave filter with true negative taps based on differential photo detection.

The light wave from an optical source is modulated by a microwave signal under processing using an intensity modulator. The modulated signal is then divided by a 1 ×2 optical coupler and delayed by the optical delay lines. The time delayed signals are sent to a balanced PD. The balanced PD consists of two matched PD with inverting biased voltage. The output signal from the two PDs is then combined and subtracted in the electrical domain. The differential detection would lead to a positive tap coefficient and a negative tap coefficient. The scheme to achieve positive and negative tap coefficients by using differential photo detection is illustrated Fig. 3.5, where a filter with two taps (one positive and one negative) is shown. The filter can be easily extended to have multi-taps by replacing the time delay device with the optical time delay array shown in Fig. 3.3.

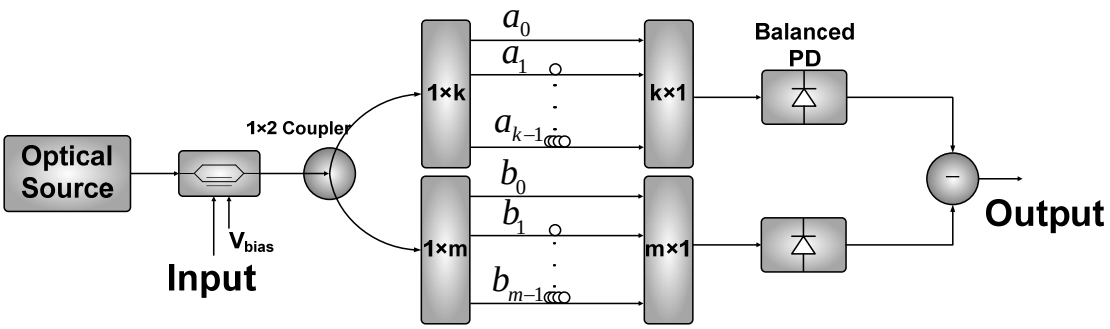

Fig. 3.6 System configuration of a photonic microwave filter with multiple positive and negative taps using differential photo detection.

The illustration of a photonic microwave filter with k positive taps and m negative taps is shown in Fig. 3.6. The positive tap coefficients are [a_0, a_1, ⋯, a_{k-1}] and the negative tap coefficients are [b_0, b_1, ⋯, b_{k-1}]. The total time delay of each tap can be easily tuned through adjusting the optical delay line. Since the negative taps are generated in the electrical domain, the filter is not all-optical, which may increase the complexity of the system.

Many techniques have been reported to implement a photonic microwave filter with positive and negative tap coefficients all optically. One solution is to use wavelength conversion based on cross-gain modulation in a semiconductor optical amplifier (SOA) [54], as shown in Fig. 3.7.

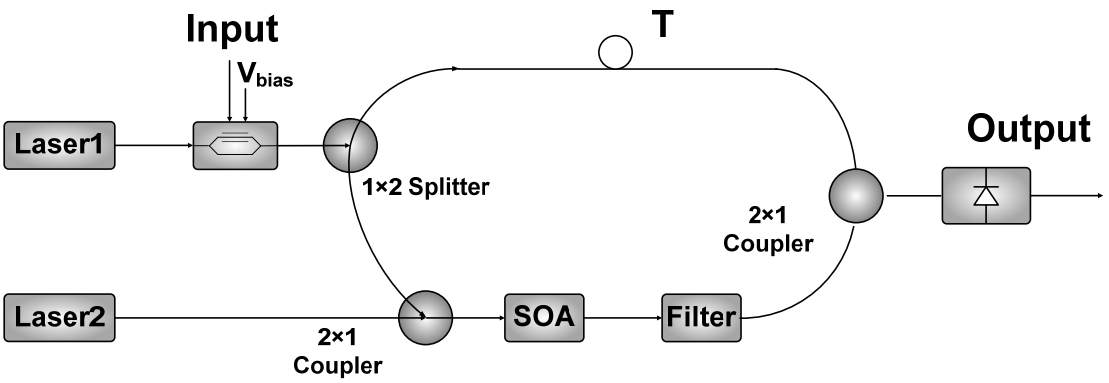

Fig. 3.7 System configuration of a photonic microwave filter with one positive and one negative taps based on cross-gain modulation in an SOA.

A light wave at λ_1 from laser 1 is modulated by the microwave signal to be processed and then split into two branches by an optical power splitter. In the upper branch, the modulated signal is time-delayed by an optical delay line. In the lower branch, the modulated optical signal and the continuous wave beam at λ_2 from laser 2 are combined together and fed to a SOA. Due to the cross-gain modulation effect, the light wave at λ_2 is modulated by the microwave modulation signal but with a π phase shift compared with the microwave signal at λ_1. An optical filter, such as a uniform FBG, is then used to block the optical signal at λ_1. The modulated signal at λ_1 from the upper branch and the modulated signal at λ_2 with a π phase shift from the lower branch are combined by a 2×1 optical coupler and sent to a PD. A photonic microwave filter with one positive and one negative tap is achieved.

Another technique to achieve a photonic microwave filter with positive and negative tap coefficients can be realized using a pair of Mach-Zehnder modulators (MZMs)

that are biased at the positive and negative linear slopes of the transfer functions to achieve amplitude inversion [56]. The system configuration of a photonic microwave filter with one positive and one negative taps using two MZMs is shown in Fig. 3.8.

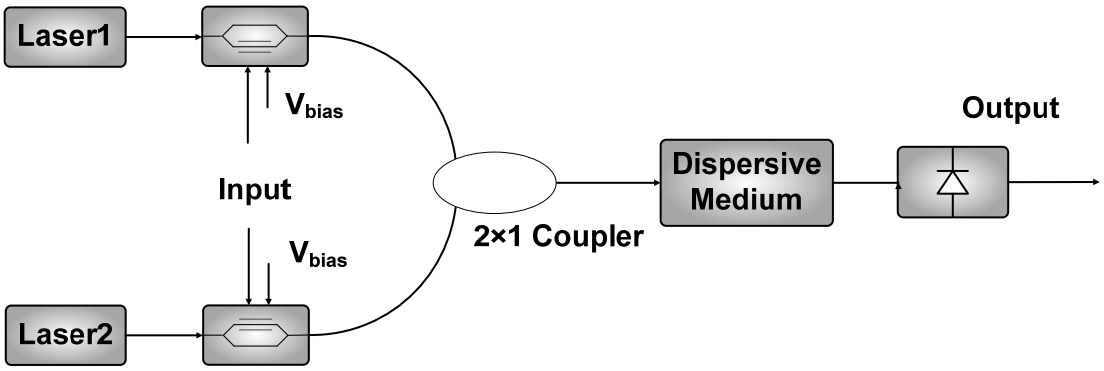

Fig. 3.8 System configuration of a photonic microwave filter with one positive and one negative taps using two MZMs biased at the positive and negative linear slopes of the transfer functions

A continuous wave at λ_1 from laser 1 is modulated by the input microwave signal at an intensity modulator which is biased at the center of the positive slope of the transfer function. Since the modulation signal is applied to the positive slope of the transfer function, the optical signal at the output of the modulator is in phase with the modulation signal. In the lower branch, the continuous wave at λ_2 is modulated by the same microwave signal but at an intensity modulator which is biased at the center of the negative slop of the transfer function. In this case, the modulation microwave signal is applied to the negative slope of the transfer function. Thus, the output signal at the output of the intensity modulator would have a π phase shift compared with the modulation signal. The signals from the two branches are combined together and sent to a dispersive medium which can be a length of SMF, a LC-FBG or a length of

DCF. The optical signals at the two wavelengths are dispersed and separated temporally. By carefully choosing the GVD of the dispersive medium and the wavelength space between λ_1 and λ_2, one can easily control the time delay between the two taps of the filter, and thus the FSR of the filter.

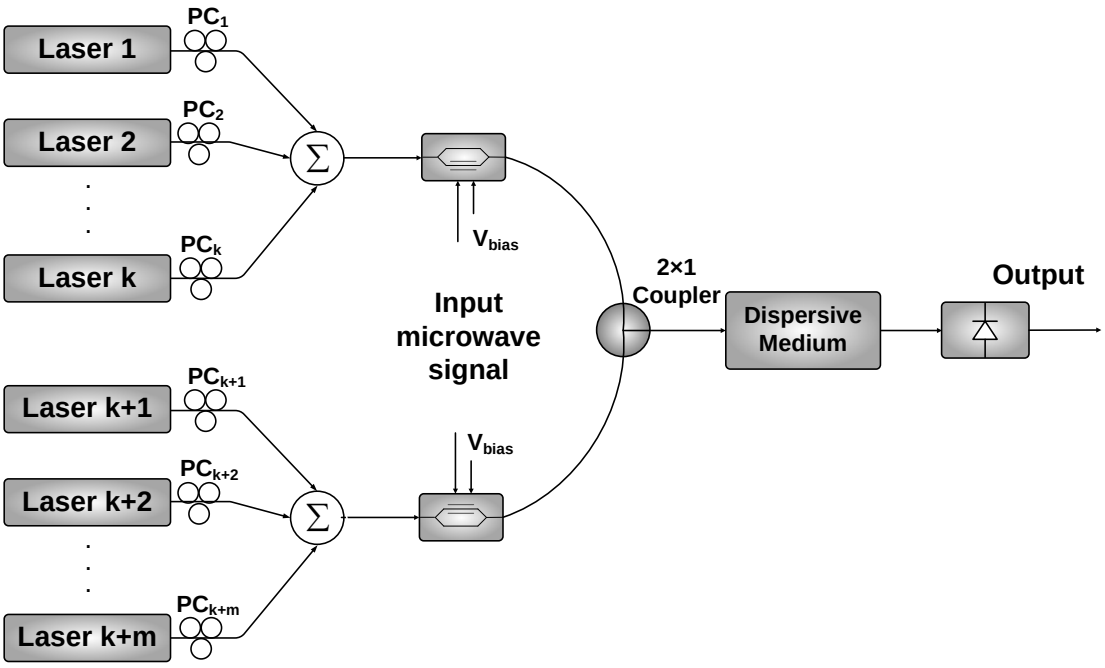

Fig. 3.9 System configuration of a photonic microwave filter with *k* positive and *m* negative taps using two MZMs biased at the positive and negative slopes of he transfer functions..

The key advantage of this technique is the flexibility to add new taps to this filter. As shown in Fig. 3.9, the filter can be simply extended to have *k* positive taps and *m* negative taps by employing *k* + *m* laser sources. The time delay between the adjacent taps is chosen by carefully designing the wavelength spacing and the GVD of the dispersive medium. The magnitudes of the tap coefficients can be controlled by controlling the output powers of the laser sources.

An incoherent photonic microwave filter with positive and negative tap coefficients can be implemented using the techniques discussed above, and a bandpass spectral response can be achieved. However, to implement a photonic microwave filter with arbitrary spectral response, a photonic microwave filter with complex coefficients is highly desirable. With a photonic microwave filter having complex coefficients, the zeros and poles of the filter can be rotated around the origin, or in other words, the shape of the frequency response can be kept unchanged while the FSR of the filter is changed.

In [58], an incoherent photonic microwave filter with complex coefficients is realized in the optical domain. The system configuration of a two-tap filter with a complex tap coefficient is shown in Fig. 3-10. The system is based on a tunable optically induced RF phase shift that is achieved by a combined use of optical single-sideband modulation (SSB) and stimulated Brillouin scattering (SBS).

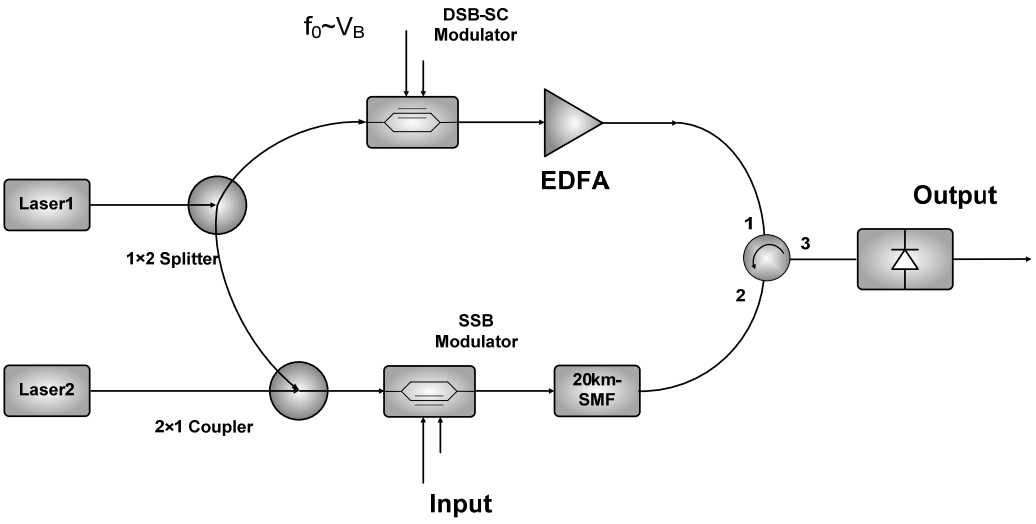

Fig. 3.10 System configuration of a photonic microwave filter with complex coefficients.

As shown in Fig. 3.10, two light waves at λ_1 and λ_2 from two laser sources are combined using a 2×1 coupler and fed to an SSB modulator. The combined optical signal is modulated by the microwave signal to be processed. The optical signal at the output of the modulator propagates through a length of SMF which separates the optical signal at two wavelengths temporally. The upper branch of the system in Fig. 3.10 is dedicated to supply the complex coefficient of the filter by inducing a phase shift to the optical carrier at λ_1. The phase shift can be tuned by controlling the modulation sinusoidal microwave signal applied to the double-sideband suppressed-carrier (DSB-SC) modulator which is a MZM biased at the minimum transmission point.

3.4 Photonic microwave filter with nonuniformly spaced taps

A photonic microwave filter with complex coefficients can have an arbitrary spectral response, which is highly needed for advanced signal processing. Although the schemes in [58] can provide complex coefficients, the implementation is extremely complicated, especially when the number of taps is large. To solve this problem, a concept to design and realize a bandpass microwave photonic filter with equivalent negative or complex tap coefficients was recently proposed [60] [61]. Instead of using uniformly spaced taps, the filter has a structure with nonuniformly spaced taps. Compared with a filter with uniformly spaced taps, in a nonuniformly spaced filter, each tap has an additional time delay, corresponding to an additional phase shift,

making the coefficient of the specific tap have an equivalent negative or complex coefficient. Based on this concept, advanced signal processing functions, such as phase coding, chirped microwave signal generation and chirped pulse compression have been demonstrated [11].

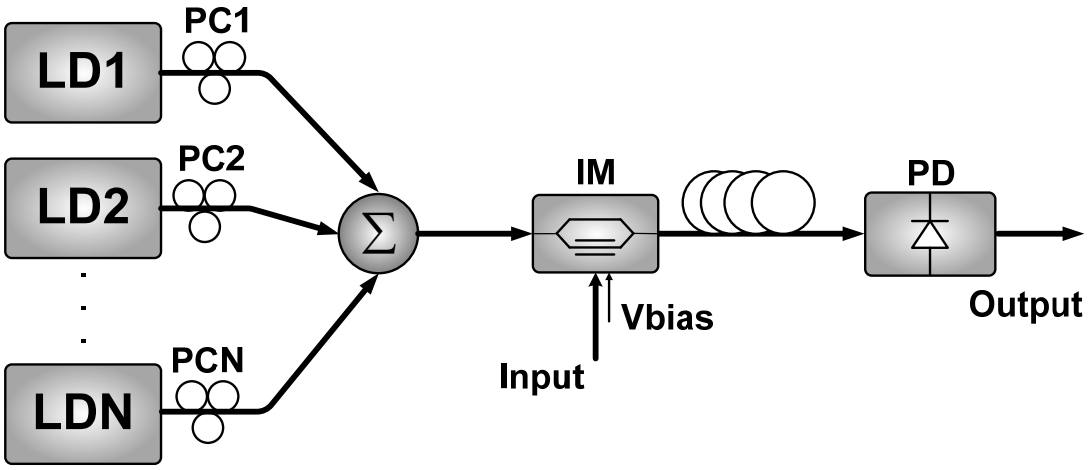

Fig. 3.11 System configuration of an *N*-tap photonic microwave filter with nonuniformly spaced taps.

As shown in Fig. 3.11, a photonic microwave filter with nonuniformly spaced taps has a configuration similar to that of a photonic microwave filter with uniformly spaced taps. The nonuniform spacing is implemented using multi-wavelength source with nonuniform wavelength spacing and a single dispersive element.

The impulse response of a regular FIR filter can be written as

$$h(t) = \sum_{n=0}^{M-1} a_n \delta(t - nT) \tag{3-7}$$

where M is the taps number, a_n is the tap coefficient of n-th tap, T is the time delay between adjacent taps and $\Omega = 2\pi/T$ is the FSR of the filter. The center frequency of the m-th channel of the filter is $m\Omega$. It is known that an FIR filter has a spectral response with multiple channels and adjacent channels are separated by the FSR of the filter. For example, if the first channel of the filter is used and the FSR of the filter is set to be 10 GHz, the time delays between adjacent taps are $\Delta\tau$ = 1/10 GHz = 100 ps.

The frequency response of a regular FIR filter with uniformly spaced taps can be calculated through FT

$$H(\omega) = \sum_{n=0}^{M-1} a_n \exp\left(-jn\frac{2\pi}{\Omega}\omega\right) \tag{3-8}$$

If an additional time delay $\Delta\tau_n$ is introduced to the n-th tap, the filter become nonuniformly spaced. The frequency response of a nonuniformly spaced filter is given by [60]

$$H_{nuni}(\omega) = \sum_{n=0}^{M-1} a_n \exp\left[-j\left(n\frac{2\pi}{\Omega} + \Delta\tau_n\right)\omega\right] \tag{3-9}$$

The frequency response around $m\Omega$ can be approximated as

$$H_{nuni}(\omega) \approx \sum_{n=0}^{M-1} a_n \exp\left(-jm\Omega\Delta\tau_n\right) \cdot \exp\left(-jn\frac{2\pi}{\Omega}\omega\right) \tag{3-10}$$

As can be seen from (3-10), the equivalent phase shift introduced by the additional time delay $\Delta\tau_n$ at around $m\Omega$ is given by

$$\phi_n = -\Delta\tau_n \times m\Omega \tag{3-11}$$

If the magnitude tap coefficients are set to be positive, the desired phase of the *n*-th tap ϕ_n can be equivalently realized by the total time delay, of *n*-th tap, which is given by

$$\tau_n = \tau_0 + nT - \frac{\phi_n}{m\Omega} \tag{3-12}$$

where τ_0 is the time delay of the first tap. Since there is a linear relationship between the wavelength spacing and the time delay difference of the adjacent filter taps, the wavelength of the *n*-th tap is given by

$$\lambda_n = \frac{\tau_n}{D \cdot L} = \lambda_0 + \frac{\tau_n - \tau_0}{D \cdot L} \tag{3-13}$$

where $\lambda_0 = \frac{\tau_0}{D \cdot L}$ is the wavelength of the first tap.

3.5 Summary

In this chapter, photonic microwave signal processing based on a microwave photonic delay-line filter was reviewed. The operation of a microwave photonic delay-line filter was presented first. Different methods to realize a photonic microwave filter with true negative and complex coefficients were summarized. Finally, the concept of using a photonic microwave filter with nonuniformly spaced taps to generate equivalent negative and complex coefficients was presented.

CHAPTER 4 PHOTONIC-ASSISTED TUNABLE MICROWAVE PULSE FRACTIONAL HILBERT TRANSFORMER BASED ON A TEMPORAL PULSE SHAPING SYSTEM

A photonic-assisted fractional Hilbert transformer with tunable fractional order, implemented based on temporal pulse shaping, is proposed and experimentally demonstrated in this chapter. The proposed fractional Hilbert transformer consists of a phase modulator and two dispersive elements with complementary dispersion. The FHT is realized if a step function is applied to the phase modulator to introduce a phase jump. The proposed technique is investigated numerically and experimentally. The results show that a real-time HT is achieved with a tunable fractional order by tuning the step function applied to the phase modulator.

4.1 Introduction

Temporal pulse shaping has been widely investigated in the past few years due to its important applications in areas such as frequency analysis [26] and arbitrary waveform generation [27]-[30]. The concept of TPS was originally proposed by Heritage and Weiner [9]. In [26], a TPS system was employed for the analysis of the spectrum of a microwave signal. Since the output in the TPS system is in the time domain, a fast measurement of the spectrum could be implemented using a real-time

oscilloscope. The most important application of the TPS technique is to achieve AWG [27]-[30]. Since the output waveform is determined by the modulation signal, the output waveform to be generated can be programmed in real time [27] [28]. In addition, the use of a TPS system incorporating a phase modulator can generate a pulse burst with tunable repetition rate [29]. Recently, it was reported that the use of a TPS system can generate a high frequency and frequency-chirped microwave waveform [30].

Due to the wide applications in modern communications and image processing, the HT is one of the most useful signal processing functions [66]. The HT can be implemented in the electrical domain using digital electronics. However, due to the limited sampling rate of the state-of-the-art digital electronics, the speed of an electronic Hilbert transformer is low. Thanks to the high frequency and large bandwidth provided by modern optics, the implementation of the HT in the optical domain would provide a solution for the processing of a high-frequency and broadband microwave signal. The HT can be implemented in the optical domain based on a phase-shifted fiber Bragg grating [41], with a bandwidth as large as a few hundred gigahertz. Recently, we proposed to implement a fractional Hilbert transformer based on a directly designed FBG using the discrete layer peeling method [42]. Since the order of the Hilbert transformer can be an arbitrary number, it provides large flexibility in signal processing. The significance of using an FBG designed based on the DLP method [42] is that the strength of the FBG was high, which would

lead to a significantly increased signal-to-noise ratio (SNR) at the output of the Hilbert transformer [42]. The major limitation of the HT using an FBG is the poor programmability. In addition, the non-flat magnitude response of the FBG will also impact the performance of the Hilbert transformer.

In this chapter, we propose and experimentally demonstrate a fractional Hilbert transformer with a tunable fractional order. The technique is achieved by using a TPS system consisting of a phase modulator and two dispersive elements with complementary dispersion. The FHT is realized if a step function is applied to the PM to introduce a phase jump to the spectrum of the microwave signal to be Hilbert transformed. The proposed technique is investigated numerically and experimentally. The results show that a real-time FHT can be achieved with a tunable fractional order by tuning the step function applied to the PM.

4.2 Principle

Generally, the standard HT of a signal $x(t)$ in the time domain is expressed as [66]

$$y(t) = x(t) * h_{HT}(t) = x(t) * \frac{1}{\pi t} \tag{4-1}$$

where $y(t)$ is the standard HT of $x(t)$, $*$ denotes the operation of convolution and $h_{HT}(t)$ is the impulse response of the standard HT filter. The expression of (4-1) in the frequency domain is

$$Y(\omega) = X(\omega) \times H_{HT}(\omega) = X(\omega) \times [-j\,\mathrm{sgn}(\omega)] \tag{4-2}$$

where $X(\omega)$ and $Y(\omega)$ are the Fourier transforms of $x(t)$ and $y(t)$, respectively, $H_{HT}(\omega)$ is the frequency response of the HT filter, and sgn(.) is the sign function.

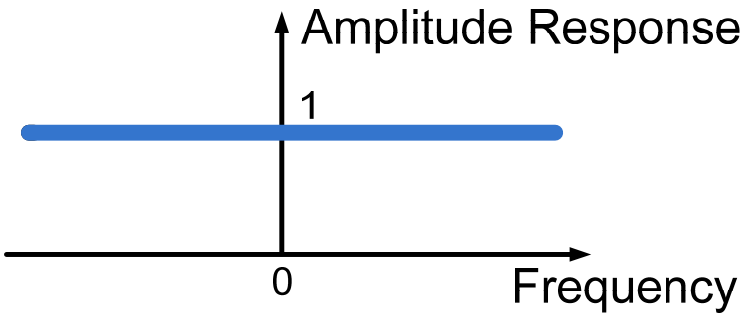

Fig. 4.1(a) Amplitude response of a fractional Hilbert transformer.

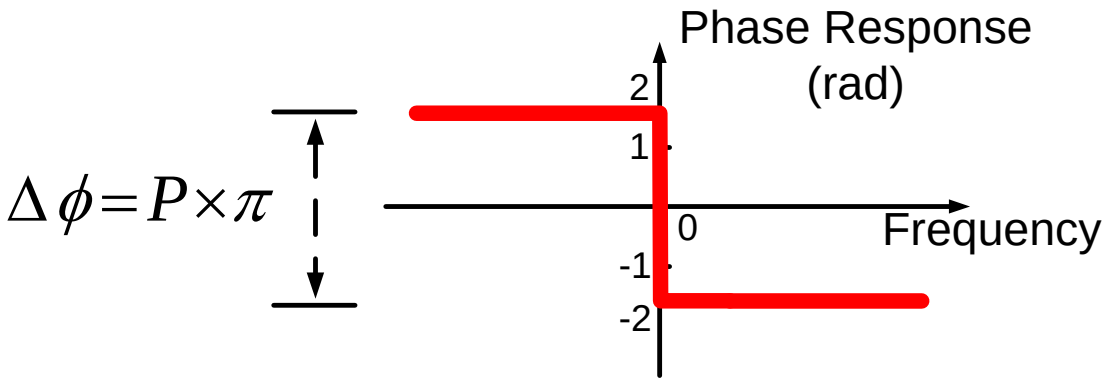

Fig. 4.1(b) Phase response of a fractional Hilbert transformer.

In order to bring in new degrees of freedom in signal analysis, the standard HT was generalized by defining a new transfer function [67]

$$H_{FHT}(\omega)=\begin{cases} e^{j\varphi}, & \omega<0 \\ e^{-j\varphi}, & \omega>0 \end{cases} \tag{4-3}$$

where $\varphi = P\times\pi/2$ and P is the fractional order. The new transform is called FHT. The amplitude and phase response a fractional Hilbert transformer is shown in Fig. 4.1 (a) and (b), respectively. Obviously, the standard HT is a special case of the FHT when the fractional order equals to 1.

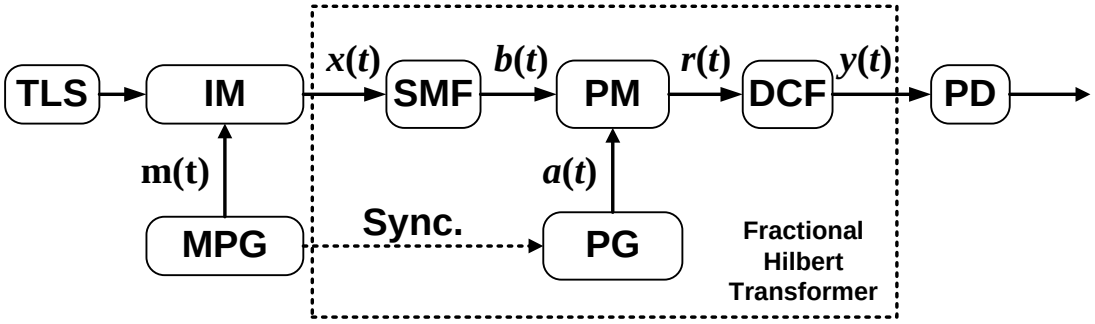

Fig. 4.2 Schematic of the TPS-based FHT system. TLS: tunable laser source; IM: intensity modulator; MPG: microwave pulse generator; SMF: single mode fiber; PM: phase modulator; PG: pattern generator; DCF, dispersion-compensating fiber; PD: photodetector.

The FHT can be implemented with a tunable fractional order using a system shown in Fig. 4.2. A microwave pulse to be processed is first modulated on an optical carrier at a MZM. Since the MZM is biased at the minimum transmission point, the envelope of the modulated signal $x(t)$ is proportional to the waveform of the microwave signal $m(t)$. Then the modulated optical signal is sent to a TPS-based fractional Hilbert transformer. The fractional Hilbert transformer consists of a phase modulator and two dispersive elements with complementary dispersion, which are a length of SMF and a

length of DCF. A step function is applied to the phase modulator to introduce a phase jump.

Mathematically, the frequency response of a dispersive medium can be characterized by

$$H_{\ddot{\Phi}}(\omega) = \left|H_{\ddot{\Phi}}(\omega)\right| \exp\left[-j\Phi\left(\omega\right)\right] \tag{4-4}$$

where $\left|H_{\ddot{\Phi}}(\omega)\right|$ is the magnitude response of the dispersive medium and $\Phi\left(\omega\right)$ is the phase response of the dispersive medium. For a dispersive medium, the magnitude response can be considered as flat within the desired bandwidth and the phase response can be expanded in Taylor series.

$$\Phi\left(\omega\right) = \Phi_0 + \dot{\Phi}\omega + \frac{1}{2}\ddot{\Phi}\omega^2 + \frac{1}{6}\dddot{\Phi}\omega^3 + \cdots \tag{4-5}$$

where Φ_0 is a constant phase, $\dot{\Phi}$ is defined as the group delay, $\ddot{\Phi}$ is defined as the group velocity dispersion and $\dddot{\Phi}$ denotes the third order dispersion (TOD). If the GVD is the main dispersive property of interest within the desired bandwidth, the frequency response of the dispersive medium in (4-4) can be approximated by

$$H_{\ddot{\Phi}}(\omega) \approx \left|H_{\ddot{\Phi}}(\omega)\right| \exp(-j\Phi_0) \exp(-j\dot{\Phi}\omega) \exp(-j\frac{1}{2}\ddot{\Phi}\omega^2) \tag{4-6}$$

where the unit of $\ddot{\Phi}$ is ps^2/rad. The impulse response of the dispersive medium can be calculated through the FT of the (4-6) by

$$h_{\ddot{\Phi}}(t) = C \exp\left[\frac{j(t-\dot{\Phi})^2}{2\ddot{\Phi}} \right] \tag{4-7}$$

where C is a constant. As can be seen from (4-7), the group delay of the dispersive medium $\dot{\Phi}$ is just a time delay. It can be ignored since it would not change the shape of the input signal. If the unit of the GVD is converted to ps^2, the impulse response of the dispersive medium is given by

$$h_{\ddot{\Phi}}(t) = C \exp\left(-\frac{j\pi t^2}{\ddot{\Phi}} \right) \tag{4-8}$$

According to (4-8), the impulse responses of the two dispersive fibers with complementary dispersion can be characterized as

$$h_{\ddot{\Phi}}(t) = C_1 \exp\left(-\frac{j\pi t^2}{\ddot{\Phi}} \right) \tag{4-9}$$

and

$$h_{-\ddot{\Phi}}(t) = C_2 \exp\left(\frac{j\pi t^2}{\ddot{\Phi}} \right) \tag{4-10}$$

where C_1 and C_2 are two constants, and $\ddot{\Phi}$ is the GVD.

Let $x(t)$ and $b(t)$ be the complex envelops of the signal at the input and the output of the SMF, respectively. Then

$$\begin{aligned} b(t) = x(t) * h_{+\ddot{\Phi}}(t) &= \int_{-\infty}^{+\infty} x(\tau) \cdot \exp\left(-\frac{j\pi(t-\tau)^2}{\ddot{\Phi}} \right) d\tau \\ &= C_1 \exp\left(-\frac{j\pi t^2}{\ddot{\Phi}} \right) \int_{-\infty}^{+\infty} x(\tau) \exp\left(-\frac{j\pi \tau^2}{\ddot{\Phi}} \right) \exp\left(\frac{j2\pi t\tau}{\ddot{\Phi}} \right) d\tau \end{aligned} \tag{4-11}$$

If the time duration of $x(t)$ is sufficiently small to satisfy

$$\left| \frac{\Delta t^2}{\ddot{\Phi}} \right| << 1 \tag{4-12}$$

where Δt is the time duration of the input pulse. Eq. (4-6) can be approximated by

$$b(t) \approx C_1 \exp\left(-\frac{j\pi t^2}{\ddot{\Phi}} \right) X(\omega)\Big|_{\omega = -\frac{2\pi t}{\ddot{\Phi}}} \tag{4-13}$$

where $X(\omega)$ is the FT of $x(t)$.

If a step function

$$a(t)=\begin{cases}-V_a, & t<0\\ V_a, & t>0\end{cases}, \tag{4-14}$$

where V_a is a constant voltage, is applied to the PM, the modulated signal at the output of the PM is given by

$$\begin{aligned} r(t) &= b(t)\cdot\exp\left(j\pi\frac{a(t)}{V_\pi}\right)\\ &= C_1\exp\left(-\frac{j\pi t^2}{\ddot{\Phi}}\right)\left\{X(\omega)\exp\left[j\varphi(\omega)\right]\right\}\Big|_{\omega=-\frac{2\pi t}{\ddot{\Phi}}} \end{aligned} \tag{4-15}$$

where V_π is the half-wave voltage of the PM and

$$\varphi(\omega)\big|_{\omega=-\frac{2\pi t}{\ddot{\Phi}}}=\begin{cases}-\pi\left(V_a/V_\pi\right), & \omega>0\\ \pi\left(V_a/V_\pi\right), & \omega<0\end{cases} \tag{4-16}$$

is the phase jump. The modulated signal is then sent to the second dispersive element. At the output of the fractional Hilbert transformer, we have

$$\begin{aligned} y(t) &= r(t)*h_{-\ddot{\Phi}}(t)\\ &= C_1C_2\int_{-\infty}^{+\infty}\exp\left(-\frac{j\pi\tau^2}{\ddot{\Phi}}\right)\left\{\Im\left[x(t)\right]\times\exp\left[j\phi(\omega)\right]\right\}\Big|_{\omega=-\frac{2\pi\tau}{\ddot{\Phi}}}\times\exp\left[\frac{j\pi(t-\tau)^2}{\ddot{\Phi}}\right]d\tau\\ &= \ddot{\Phi}C_1C_2\exp\left(\frac{j\pi t^2}{\ddot{\Phi}}\right)\Im^{-1}\left\{X(\omega)\cdot\exp\left[j\varphi(\omega)\right]\right\}\Big|_{\omega=-\frac{2\pi t}{\ddot{\Phi}}} \end{aligned} \tag{4-17}$$

where $\Im^{-1}$ denotes the operation of the inverse FT.

Again, if $\left|\Delta t^2 / \ddot{\Phi}\right| << 1$, Eq. (4-17) can be approximated as

$$\begin{aligned} y(t) &\approx C_1 C_2 \ddot{\Phi} \Im^{-1}\left\{ X(\omega) \cdot \exp\left[j\varphi(\omega) \right] \right\}\Big|_{\omega=-\frac{2\pi t}{\ddot{\Phi}}} \\ &= C_1 C_2 \ddot{\Phi} \Im^{-1}\left\{ X(\omega) \cdot H_{FHT}(\omega) \right\}\Big|_{\omega=-\frac{2\pi t}{\ddot{\Phi}}} \end{aligned} \tag{4-18}$$

It can be seen that the output waveform is a Hilbert transformed version of the input waveform. By simply tuning the amplitude of the step function applied to the PM, we can easily adjust the fractional order of the FHT filter.

If the 3-dB bandwidth of the input signal $x(t)$ is $\Delta\omega$, then the temporal width of the pulse $b(t)$ at the output of the SMF is $\Delta\omega \cdot \ddot{\Phi} / 2\pi$ [25]. Practically, the step function $a(t)$ generated by a pattern generator does not have an ideal jump at $t = 0$, and a non-zero rise time must be considered. To make the impact negligible, the rising time of the step function compared with the temporal width of the stretched pulse $b(t)$ should be sufficiently small, $\tau_r << \Delta\omega \cdot \ddot{\Phi} / 2\pi$, where τ_r is the rise time of the step function. For example, if a dispersive medium with a value of GVD of 10000 ps^2 is used and the rise time of the step function is 20 ps, the bandwidth of the pulse to be transformed should be at least 20 GHz with 10 considered as a factor for being large enough. In other words, a transform-limited Gaussian-like pulse with temporal width up to 22 ps can be accurately processed when the rise time is 20 ps. Considering that

20 ps is almost the shortest rise time that an electronic device can provide, if we want to extend the time duration of the pulse under processing, we may need to increase the GVD of the DEs to keep $\left|\Delta t^2 / \ddot{\Phi}\right| << 1$ valid. In such a case, longer SMF and DCF are needed. However, if the SMF and DCF are too long, other effects such as the TOD must be taken into consideration.

To further investigate the impact of the rise time on the performance of the proposed system, a simulation is performed. In the simulation, a 550-fs Gaussian pulse is applied to the FHT, with the rise time increased from 20 ps, the shortest rise time of an electronic device can reach as far as we know, to 800 ps, and the output waveforms are shown in Fig. 4.3. It can be seen the output waveforms become more distorted compared with the ideal waveforms with the increase of the rise time. To quantitatively evaluate the errors due to the non-zero rise time, we calculate the normalized root mean square errors (NRMSEs). For $P = 0.5$, the NRMSE is smaller than 2% for the rise times from 20 to 800 ps. For $P = 1$, the NRMSE is within 12%.

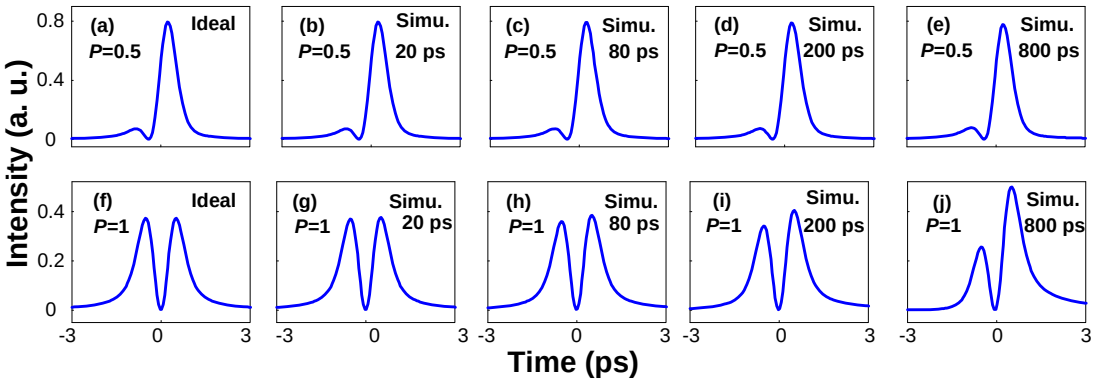

Fig. 4.3 Numerical results of an ideal FHT and a TPS-based FHT. (a) Ideal FHT with a fractional order of 0.5. The TPS-based FHT with a fractional order of 0.5 and a rise time of (b) 20 ps, (c) 80 ps, (d) 200 ps, and (e) 800 ps. (f) Ideal FHT with a fractional order of 1. The TPS-based FHT with a fractional order of 1 and a rise time of (g) 20 ps, (h) 80 ps, (i) 200 ps, and (j) 800 ps.

In the above analysis, only the GVD is considered. The impact of higher-order dispersion, mainly the TOD, is also evaluated. Higher order dispersion will impact the performance of the system, but the impact is small. The relationship between the NRMSEs of the transformed pulse and the rise time of the phase jump are shown in Fig. 4.4 (the fractional order is 0.5) and Fig. 4.5 (the fractional order is 1). The NRMSEs with perfectly matched GVD of the two dispersive medium and zero TOD are shown in Fig. 4.4(a) and Fig. 4.5(a). The NRMSEs with perfectly matched GVD and perfectly matched non-zero TOD are shown in Fig. 4.4(b) and Fig. 4.5(b). The NRMSEs with perfectly matched GVD and 5% mismatched TOD are shown in Fig. 4.4(c) and Fig. 4.5(c). According to our calculations, the NRMSE would increase when perfectly matched but non-zero TOD is taken into account, but less than 1%. However, when the GVD is perfectly matched while the TOD is mismatched, the NRMSEs will increase. For example, for a mismatch of 5% in TOD, the total NRMSE is within 13% for $P = 1$.

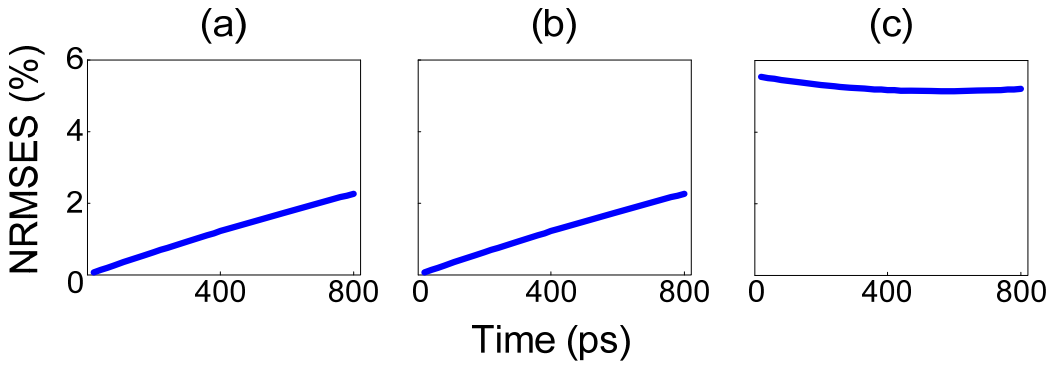

Fig. 4.4 NRMSEs for the case of a fractional order is 0.5 (a) without considering the TOD, (b) considering a non-zero and perfectly matched TOD, (c) considering the TOD with 5% mismatch.

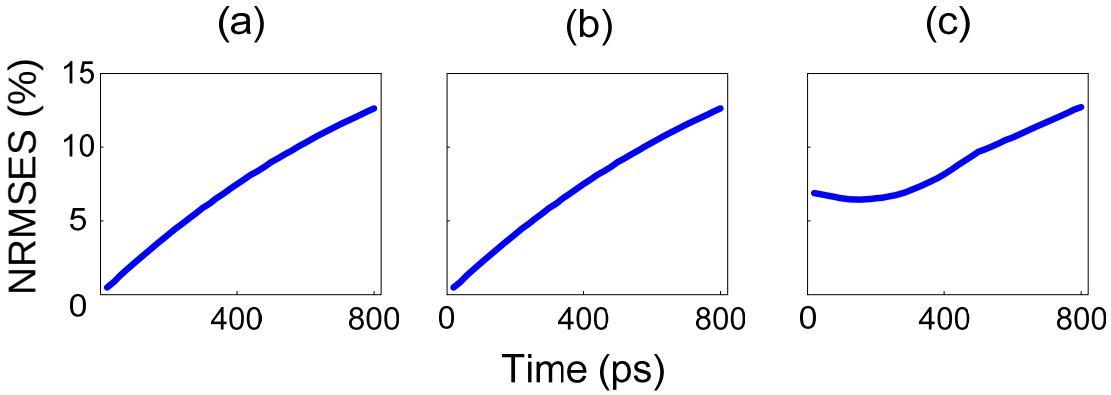

Fig. 4.5 NRMSEs for the case of a fractional order is 1 (a) without considering TOD, (b) considering a non-zero and perfectly matched TOD, (c) considering the TOD with 5% mismatch.

4.3 Simulation and experiment

A proof-of-concept experiment is then carried out based on the setup shown in Fig. 4. 2. Since a microwave pulse with a 3-dB bandwidth greater than 12.5 GHz is hard to generate, in the experiment an optical pulse from a mode-locked laser is directly employed and is applied as an input to the fractional Hilbert transformer. The 3-dB temporal width of the pulse from the MLL is 550 fs. A 36.91-km SMF (SMF1) with a

value of dispersion of -4872 ps^2 is employed to stretch the pulse from the MLL, and the stretched pulse is sent to a PM. The PM has a half-wave voltage of 10.9 V and the 3-dB temporal pulse width of the stretched pulse is 4.9 ns. A DCF with a value of dispersion of 4872 ps^2 is connected after the PM. A step function generated by an arbitrary waveform generator (Tektronix AWG7102) and amplified by a microwave amplifier is applied to the PM via the RF port. A Hilbert transformed pulse is thus obtained at the output of the DCF.

Since the pulse at the output of the DCF has a temporal width of only several picoseconds, it is too fast to be detected by a photodetector. To monitor the output pulse, another 6.74-km SMF (SMF2) with a value of dispersion of -890 ps^2 is used to stretch the output pulse, to make it wide enough to be detected by the PD. In addition, the transformed pulse would also be distorted during the stretching process. The distortion is also considered in the simulation shown in Fig. 4.6.

The experimental results for the fractional Hilbert transformer with different fractional orders of 0.41, 0.52 and 0.71 are shown in Fig. 4.6. Simulation results by taking into consideration of the additional 6.74-km SMF are also shown as a comparison. The experimental results agree well with the results by the simulations. Note that a 20-GHz electro-optic PM with an ultralow half-wave voltage of 3 V at 1 GHz is commercially available. If such a PM is employed, a FHT with a fractional order from 0 to 2 can be easily achieved.

The rise time of the step functions for the three different fractional orders is 63.3 ps, which is small and has negligible impact on the FHT. The NRMSEs of the three experimentally obtained pulses in Fig. 4. 6(a), (b) and (c) are 4.24%, 3.98% and 3.87%, respectively.

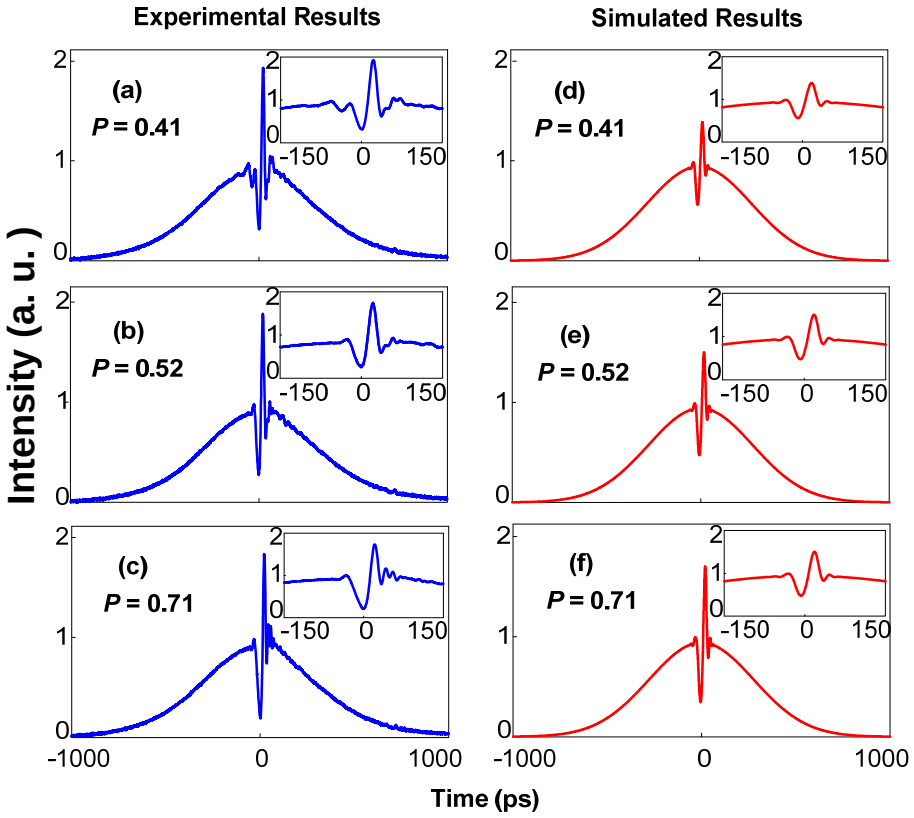

Fig. 4.6 Experimental results for the fractional orders of (a) 0.41, (b) 0.52, and (c) 0.71. The experimental results are compared with the simulation results (d), (e) and (f).The details of the central portion are shown in each inset.

4.4 Discussion and conclusion

The implementation of a photonic-assisted microwave pulse fractional Hilbert transformer with tunable fractional order based on TPS was proposed and experimentally demonstrated. The fractional Hilbert transform was realized by introducing a phase jump to the spectrum of the input pulse via phase modulation and the tunability of the fractional order was achieved by changing the amplitude of the step function applied to the PM. The key advantage of this technique is its flexibility in changing the fractional order, which may find applications where a Hilbert transform with a tunable order is needed. Hilbert transform can be found in wide applications in modern communication, radar and image processing systems [66].

Based on the theoretical analysis in Chapter 2, arbitrary phase and magnitude response can be imposed to the input ultrashort optical pulse by employing a PM and an IM, respectively. Thus, a filter with an arbitrary frequency and phase response can be achieved using a TPS system with both PM and an IM. A boardband photonic differentiator can also be achieved using the TPS system. In this case, two channels of signal are needed to apply on the IM and the PM, respectively. However, the synchronization among the MLL, the channel for the IM and the channel for the PM is hard to achieve. Thus, TPS is especially for the applications where a single modulator is needed, for example, a Hilbert transformer where only a PM is needed and a symmetrical waveform generator where only an IM is needed [27].

CHAPTER 5 A MICROWAVE BANDPASS DIFFERENTIATOR IMPLEMENTED BASED ON A NONUNIFORMLY-SPACED PHOTONIC MICROWAVE DELAY-LINE FILTER

A microwave bandpass differentiator implemented based on a finite impulse response (FIR) photonic microwave delay-line filter with nonuniformly-spaced taps is proposed and experimentally demonstrated. To implement a microwave bandpass differentiator, the coefficients of the photonic microwave delay-line filter should have both positive and negative coefficients. In the proposed approach, the negative coefficients are equivalently achieved by introducing an additional time delay to each of the taps, leading to a π phase shift to the tap. Compared with a uniformly-spaced photonic microwave delay-line filter with true negative coefficients, the proposed differentiator features a greatly simplified implementation. A microwave bandpass differentiator based on a six-tap nonuniformly-spaced photonic microwave delay-line filter is designed, simulated, and experimentally demonstrated. The reconfigurability of the microwave bandpass differentiator is experimentally investigated. The employment of the differentiator to perform differentiation of a bandpass microwave signal is also experimentally demonstrated.

5.1 Introduction

Microwave signal processing based on photonic techniques has been a topic of interest in the past few years [4]. Due to the limited speed of the currently available digital electronics, the processing of high-frequency and broadband signal based on photonic techniques has been considered a promising solution. Among the numerous signal processing schemes, the one based on a delay-line architecture with a FIR has been widely investigated, which can find applications such as spectral filtering, phase coding, chirped microwave signal generation, and chirped pulse compression. To avoid optical interference, a photonic microwave delay-line filter is usually operating in the incoherent regime. The major limitation of a photonic microwave delay-line filter operating in the incoherent regime is that the tap coefficients are all positive, which makes the FIR delay-line filter a low-pass only. For many applications, however, a bandpass filter with negative or complex coefficients is needed [4].

Numerous techniques have been proposed to achieve a photonic microwave delay-line filter with positive and negative tap coefficients [54]-[57]. A microwave photonic filter with positive and negative coefficients can be implemented based on cross-gain modulation (XGM) [54] or cross-polarization modulation (XPolM) [55] in a SOA. Positive and negative tap coefficients can also be realized using a pair of MZMs that are biased at the positive and negative linear slopes of the transfer functions to achieve amplitude inversion [56]. A pair of positive and negative tap coefficients can be generated based on phase modulation and phase-modulation to

intensity-modulation conversion by passing the phase-modulated optical signal through a pair of CFBGs with complementary GVD responses [57]. Photonic microwave delay-line filters with complex tap coefficients have also been proposed [58] [59]. In [58], a complex coefficient is generated by introducing a phase shift to the microwave signal to be processed, which is realized based on a combined use of optical single-sideband modulation (SSB) and stimulated Brillouin scattering (SBS). In [59], a complex coefficient is generated using a wideband tunable optical microwave phase shifter that consists of two electro-optic MZMs. A continuous tuning of a phase shift from -180^{o} to $+180^{o}$ was demonstrated. A comprehensive review of photonic microwave filters with negative or complex coefficients can be found in [2].

A photonic microwave delay-line filter with complex coefficients can have an arbitrary spectral response, which is highly needed for advanced signal processing. Although the schemes in [58] [59] can provide complex coefficients, the implementation is extremely complicated, especially when the number of taps is large. To solve this problem, we have recently developed a concept to design and realize a bandpass microwave photonic delay-line filter using equivalent negative or complex tap coefficients [60] [61] with nonuniformly-spaced taps. By introducing an additional time delay to a tap, an additional phase shift will be introduced to the tap coefficient, making the tap have an equivalent negative or complex coefficient. Based on this concept, advanced signal processing functions, such as phase coding, chirped

microwave signal generation and chirped pulse compression, have been demonstrated [61].

Due to the wide applications in radar and modern communication systems, temporal differentiation is one of the most important signal analyzing and processing functions. A temporal differentiator can be implemented using digital electronics, but at a lower speed and narrower wideband compared with the implementation in the optical domain. Numerous photonically assisted temporal differentiators have been proposed and demonstrated. A temporal differentiator could be achieved using a π PS-FBG [37], a long-period fiber grating [38], or a special FBG designed using the DLP method [39]. A temporal differentiator could also be achieved based on PM and PM-IM conversion in an FBG serving as a frequency discriminator [68] [69]. A temporal differentiator using other schemes such as the XGM [70] and the XPolM [71] in a SOA has also been reported.

In this chapter, we propose and experimentally demonstrate a microwave bandpass differentiator based on a photonic microwave delay-line filter. A first-order bandpass temporal differentiator has a transfer function of the form given by $\mathrm{j}(\omega-\omega_0)$, where ω_0 is the angular frequency of the microwave carrier, which can be implemented using a photonic microwave delay-line filter with a linear magnitude response within the bandwidth and a π phase shift at ω_0. A photonic microwave delay-line filter with such a spectral response should have both positive and negative coefficients [72].

The techniques proposed for the generation of negative coefficients in [54]-[57] can be employed for the implementation of a temporal differentiator, but the system is very complicated and costly. In this chapter, we propose to implement a temporal differentiator based on a photonic microwave delay-line filter with nonuniformly-spaced taps. The negative taps are equivalently achieved through nonuniform spacing. A microwave bandpass differentiator based on a six-tap nonuniformly-spaced microwave delay-line filter is designed. Its performance is evaluated based on numerical simulations. An experimental demonstration of the differentiator is also performed. The reconfigurability of the differentiator is investigated. The differentiation of a bandpass microwave signal using the differentiator is also experimentally demonstrated.

The remainder of the chapter is organized as follows. In 5.2, the principle of a microwave bandpass differentiator based on a nonuniformly-spaced photonic microwave delay-line filter is presented. A microwave bandpass differentiator based on a six-tap nonuniformly-spaced photonic microwave delay-line filter is designed and its performance is evaluated based on numerical simulations. In 5.3, a proof-of-concept experiment is performed, in which a microwave bandpass differentiator based on a six-tap nonuniformly-spaced photonic microwave filter is demonstrated. In 5.4, the differentiation of a bandpass microwave signal using the differentiator is experimentally demonstrated. In 5.5, a conclusion is drawn.

5.2 Principle

A temporal differentiator can be implemented using a filter having a frequency response given by

$$H_D(\omega) = j(\omega - \omega_0) = \begin{cases} (\omega - \omega_0)e^{j\frac{\pi}{2}} & (\omega - \omega_0) > 0 \\ -(\omega - \omega_0)e^{j\left(-\frac{\pi}{2}\right)} & (\omega - \omega_0) < 0 \end{cases} \tag{5-1}$$

where ω_0 is the angular frequency of the microwave carrier. From (5-1) we can see that the temporal differentiator has a linear magnitude frequency response and a π phase jump at $\omega = \omega_0$. Considering that a differentiator should always have a finite bandwidth, the transfer function can be further defined by applying a window function, with the magnitude response shown in Fig. 5.1, where a window function with a width of 2 GHz is applied to the magnitude response.

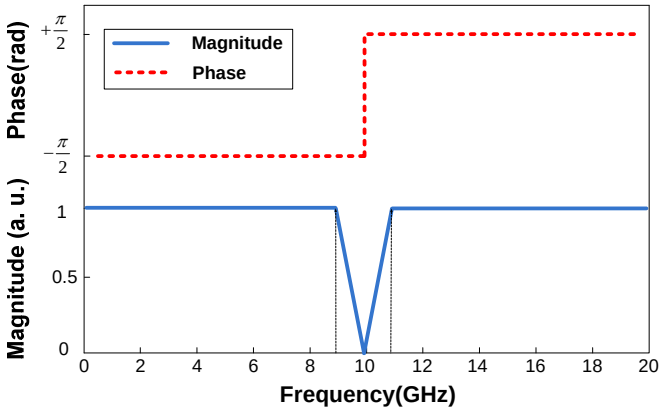

Fig. 5.1 The frequency response of a bandpass microwave differentiator.

The impulse response of a temporal differentiator implemented based on a regular FIR filter can be written by

$$h(t) = \sum_{n=0}^{N-1} a_n \delta(t - nT) \tag{5-2}$$

where N is the number of taps, a_n is the tap coefficient of the n-th tap, and T is the time delay between adjacent taps. If we apply Fourier transform to (5-2), we have the frequency response of the FIR filter,

$$H(\omega) = \sum_{n=0}^{M-1} a_n e^{-j\omega nT} \tag{5-3}$$

From (5-3) we can see that the FIR filter has multiple spectral channels and any adjacent channels are separated by a FSR given by $\Omega = 2\pi/T$. The center frequency of the m-th channel of the filter is $m\Omega$. If the FSR of the filter is set to be 9.95 GHz, the time delay between adjacent taps is $T = 100.5$ ps.

The impulse response of a regular FIR filter with six uniformly-spaced taps to achieve the frequency response shown in Fig. 5.1 can be calculated through the Remez algorithm [72], with the coefficients shown in Fig. 5.2(a). As can be seen the tap coefficients have both positive and negative values. The implementation of the microwave photonic delay-line filter using the regular uniformly-spaced FIR structure

will make the system extremely complicated. A solution to simplify the implementation is to use the structure having nonuniformly-spaced taps.

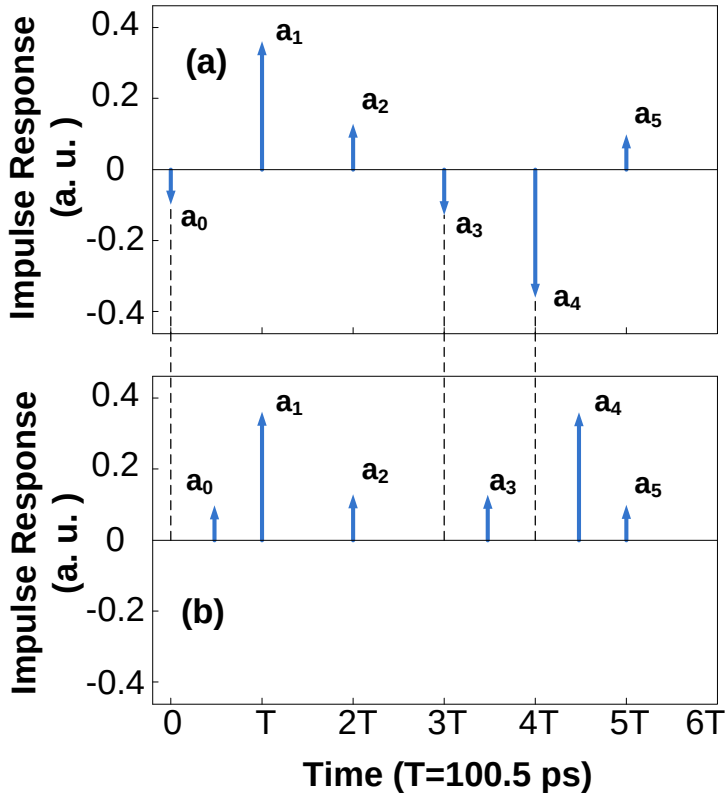

Fig. 5.2 Design of the temporal differentiator based on a six-tap FIR filter. (a) Impulse response of the six-tap uniformly-spaced FIR filter. (b) Impulse response of the six-tap nonuniformly-spaced FIR filter.

If an additional time delay $\Delta\tau_n$ is introduced to the *n*-th tap, the filter becomes a nonuniformly-spaced FIR filter [59]. The frequency response is given

$$H_N(\omega) = \sum_{n=0}^{M-1} a_n \cdot \exp\left(-j\left(n\frac{2\pi}{\Omega} + \Delta\tau_n\right)\omega\right) \tag{5-4}$$

Assume the passband of interest is narrow and the central frequency is $m\Omega$, then the frequency response in (5-4) can be approximated as

$$H_N(\omega) \approx \sum_{n=0}^{M-1} a_n \exp\left(-jm\Omega\Delta\tau_n\right) \cdot \exp\left(-jn\frac{2\pi}{\Omega}\omega\right) \tag{5-5}$$

where we have $\exp\left(-j\omega\Delta\tau_n\right) \approx \exp\left(-jm\Omega\Delta\tau_n\right)$.

An equivalent phase shift introduced by the additional time delay $\Delta\tau_n$ at the passband of interest is

$$\phi_n \approx -\Delta\tau_n \times m\Omega \tag{5-6}$$

If the FIR filter is implemented using all positive coefficients, the phase term of *n*-th tap ϕ_n can be equivalently realized by the an additional time delay, with the time delay of the *n*-th tap given by

$$\tau_n = nT - \frac{\phi_n}{m\Omega} \tag{5-7}$$

Based on (5-7), an FIR filter with all-positive coefficients to achieve the same function as a regular FIR filter can be designed. Fig. 5.2(b) shows the tap coefficients of a six-tap FIR filter with nonuniformly-spaced taps for the implementation of the microwave bandpass differentiator shown in Fig. 5.1. It can be seen from Fig. 5.2(b) that the tap coefficients are all positive, but with nonuniformly spaced taps.

The frequency responses of the six-tap FIR filter with uniformly and nonuniformly spaced taps are shown in Fig. 5.3(a) and (b). As can be seen from Fig. 5.3(a), the filter

has a linear magnitude response within the 2-GHz bandwidth from 8.96 to 10.95 GHz and a π phase jump at the center frequency of 9.95 GHz. The frequency response of the nonuniformly-spaced FIR filter is shown in Fig. 5.3(b). Within the 2-GHz bandwidth from 8.96 to 10.95 GHz, the magnitude response of the filter is approximately linear, and a π phase jump also occurs at the center frequency of 9.95 GHz.

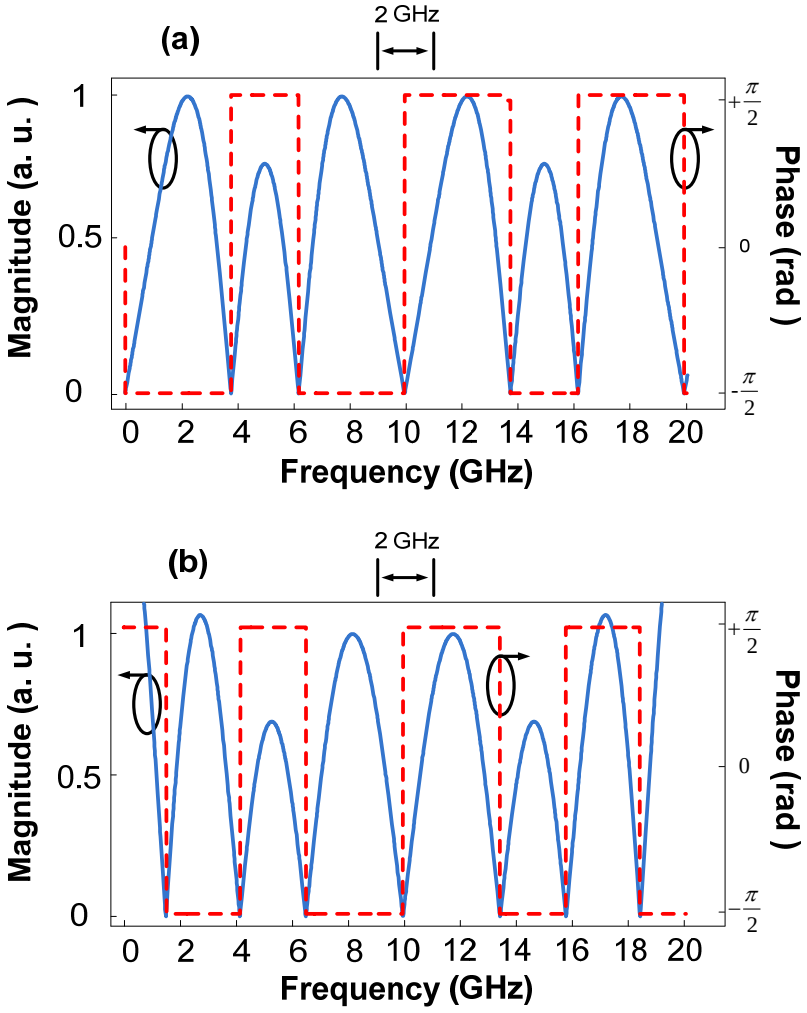

Fig. 5.3. Frequency response of a differentiator based on a six-tap uniformly-spaced and nonuniformly-spaced FIR filter. (a) Frequency response of the six-tap FIR filter with uniformly-spaced

taps. (b) Frequency response of the six-tap nonuniformly-spaced FIR filter with nonuniformly-spaced taps.

If we compare the frequency responses in Fig. 5.3(a) and (b), we can see that the frequency response of the regular FIR filter is periodic and any two adjacent channels are separated by the FSR of the filter. However, the frequency response of the nonuniformly spaced FIR filter is aperiodic. The aperiodicity is resulted due to the fact that the phase shift is introduced based on an additional time delay, which is frequency dependent. The phase shift is accurate only for the frequency at $m\Omega$ and approximately accurate at the passband centered at $m\Omega$ [59]. To ensure an accurate phase shift in the passband of interest, the filter should have a narrow bandwidth. The filter shown in Fig. 5.3(b) is designed to have a bandwidth of 2 GHz, the normalized root mean square (NRMS) error between the magnitude responses shown in Fig. 5.3(a) and (b) within the 2-GHz bandwidth is calculated to be 2.44%, which is very small. Therefore, it is feasible to implement a differentiator using a nonuniformly spaced photonic microwave delay-line filter, with a significantly reduced complexity.

5.3 Simulation and experiment

A proof-of-concept experiment is then carried out to demonstrate the microwave bandpass differentiator based on the six-tap nonuniformly spaced FIR filter. The center frequency is 9.95 GHz, and the bandwidth is 2 GHz from 8.96 GHz to 10.95 GHz.

Based on the Remez algorithm, the tap coefficients of a regular six-tap microwave photonic FIR filter are calculated to be [-0.099, 0.362, 0.129, -0.129, -0.362, 0.099]. The implementation is complicated due to the three negative values of the tap coefficients. If the differentiator is implemented using a nonuniformly-spaced microwave photonic delay-line filter, the coefficients can be all positive, with the negative coefficients equivalently achieved by additional time delays. Based on (5-5), the tap coefficients are [0.099, 0.362, 0.129, 0.129, 0.362, 0.099] and the time delays for the six taps are [0.5*T*, *T*, 2*T*, 3.5*T*, 4.5*T*, 5*T*], where *T* is the time delay difference two between adjacent taps in a regular uniformly-spaced FIR filter, which is 100.5 ps.

Fig. 5.4 shows the experimental setup to implement the six-tap nonuniformly-spaced microwave photonic delay-line filter. The six taps are generated using six wavelengths with identical wavelength spacing. When the six wavelengths are traveling through a dispersive element, an identical time delay different between any two adjacent wavelengths is generated. In the experiment, the six wavelengths are generated by a laser array, which are multiplexed using an optical coupler and sent to an IM which is biased at the linear transmission point. Six PCs are used to adjust the polarization directions of the light waves to minimize the polarization dependent loss at the IM. A 9.8-km SMF connected at the output of the IM is used to serve as a dispersive element. Assume that the first wavelength is λ_0 and the *n*-th wavelength is λ_n, the time delay for the *n*-th tap due to the dispersive element is given by

$\tau_n = D(\lambda_n - \lambda_0)L$, where D is the chromatic dispersion parameter of the SMF and L is the length of the SMF. If λ_0 is given, the n-th wavelength is calculated by

$$\lambda_n = \lambda_0 + \frac{\tau_n}{D \cdot L} = \lambda_0 + \frac{nT - \phi_n / m\Omega}{D \cdot L} \tag{5-8}$$

The six wavelengths are $\lambda_0 + [0, 0.5, 1.5, 3, 4, 4.5] \cdot \Delta\lambda$, where $\Delta\lambda = T/D \cdot L$ is the wavelength spacing of two adjacent wavelengths corresponding a regular uniformly spaced FIR filter.

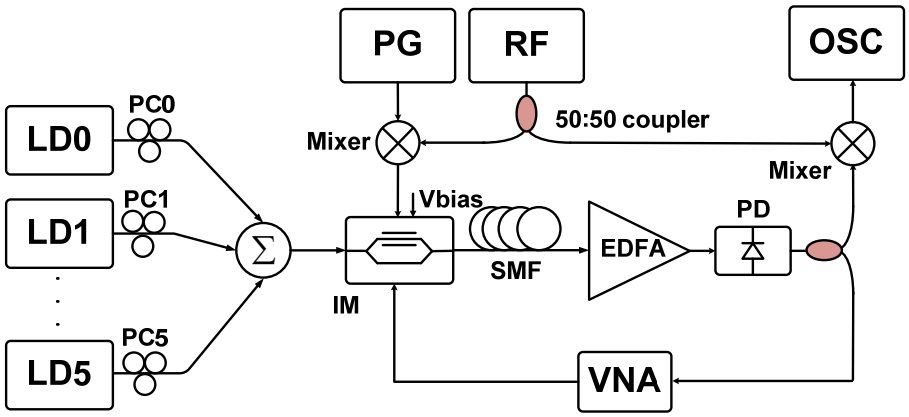

Fig. 5.4 Experimental setup for the implementation of a photonic microwave differentiator based on a six-tap nonuniformly-spaced delay-line filter. PC: polarization controller; VNA: vector network analyzer; EDFA: erbium-doped fiber amplifier; PG: pulse generator; RF: radio frequency source; OSC: real-time oscilloscope, PD: photodetector.

For a standard SMF, the chromatic dispersion parameter is D = 17 ps/nm/km. In the experiment, the first wavelength is selected to be 1543.860 nm, based on (5-8) the other five wavelengths are calculated to be 1544.160, 1544.760, 1545.660, 1546.260, and 1546.560 nm. The spectrum of the six-wavelength laser array is measured and

shown in Fig. 5.5(a). The measured magnitude and phase responses of the differentiator are shown in Fig. 5.5(b) and (c), respectively. The center frequency of the passband is measured, which is 9.95 GHz. The simulated magnitude and phase response of the six-tap FIR filter with uniformly-spaced taps generated by the same filter coefficients are also shown in Fig. 5.5(b) and (c) for comparison. The NRMS error between the experimental and simulated magnitude response shown in Fig. 5.5(b) is 2.69%, which is slightly higher than the theoretical value of 2.44%. The additional error results from the errors in the experiment. As can be seen from Fig. 5.5(c), a π phase shift also occurs at 9.95 GHz. The experimental results agree well with the simulated results.

The reconfigurability of the differentiator is then investigated. The center frequency of the differentiator is tuned to 8.53 GHz, thus the wavelength spacing corresponding to a regular uniformly spaced FIR filter is $\Delta\lambda = 0.7$ nm. As shown in Fig. 5.5 (d), the wavelengths for the six taps are 1543.860, 1544.210, 1544.910, 1545.960, 1546.660, and 1547.010 nm. The measured magnitude and phase responses are shown in Fig. 5.5(e) and (f). The measured center frequency is 8.53 GHz. The simulated magnitude and phase responses of the differentiator are also shown in Fig. 5.5(b) and (c) for comparison. The NRMS error between the simulated and experimental magnitude response is 2.71%, which is small. As can be seen from Fig. 5.5(f), a π phase shift also occurs at 8.53 GHz. The experimental results again agree well with the simulated results.

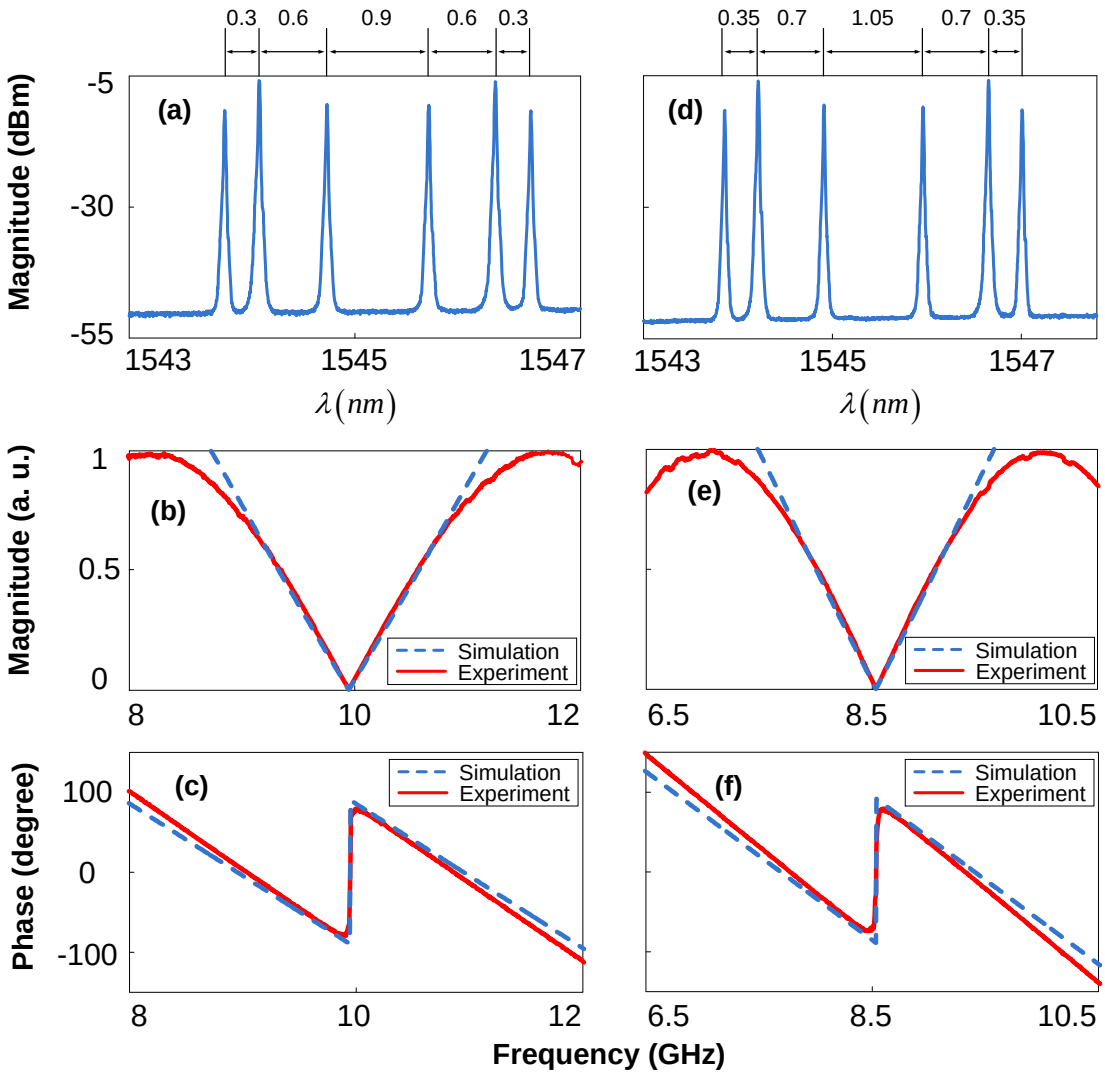

Fig. 5.5 Experimental results. (a) The measured spectrum of the six-wavelength laser array. Theoretically calculated (dashed line) and experimentally measured (solid line) (b) magnitude response of the 9.95-GHz differentiator, and (c) phase response of the 9.95-GHz differentiator. (d) The measured spectrum of the six-wavelength laser array for the differentiator with a center frequency at 8.53 GHz. Theoretically calculated (dashed line) and experimentally measured (solid line) (e) magnitude response of the 8.53-GHz differentiator, and (f) phase response of the 8.53-GHz-differentiator.

To further evaluate the microwave bandpass differentiator, the differentiation of a bandpass microwave signal is experimentally performed. In the experiment, a

Gaussian pulse is used as an input. It is known that the first-order derivative of a Gaussian pulse is a monocycle. A monocycle pulse can find applications in UWB communications [73].

A Gaussian pulse with a full-width at half-maximum (FWHM) of 270 ps generated by a pattern generator (Tektronix AWG7102), shown in Fig. 5.6(a), is mixed with a microwave carrier at 9.95 GHz generated by a microwave signal generator (Agilent E8254A), and then sent to the IM. The spectral width of the bandpass microwave signal is 1.6 GHz, which is smaller than the bandwidth of the microwave bandpass differentiator. The differentiated bandpass microwave signal is obtained at the output of the PD. To compare the original baseband waveform and the differentiated baseband waveform, a second microwave mixer is employed, to which the same microwave carrier at 9.95 GHz is applied. The differentiated baseband waveform is measured by an oscilloscope (Tektronix TDS7704B), which is shown in Fig. 5.6(b).

As a comparison, the waveform based on ideal differentiation is shown in Fig. 5.6(c). In obtaining the waveform in Fig. 5.6(c), a bandpass filter with a 3-dB bandwidth of 2 GHz is employed to remove the high-frequency noise resulted from the differentiation process. The NRMS error between the experimented and the simulated waveforms in Fig. 5.6(b) and (c) is 12.11%.

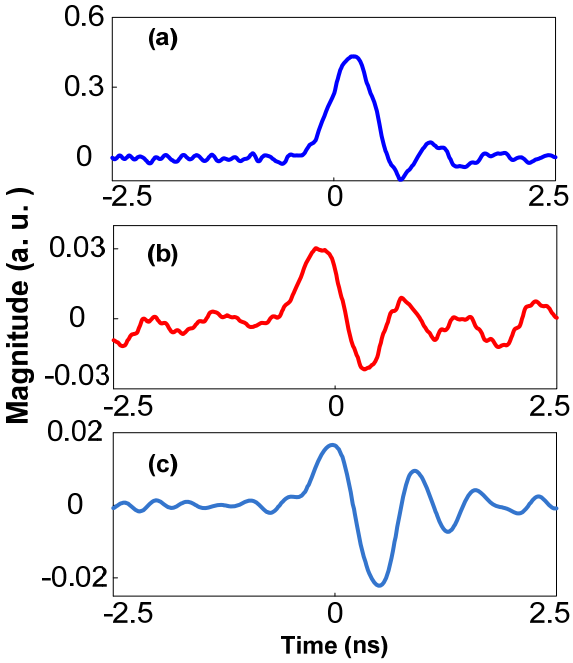

Fig. 5.6 Differentiation of a bandpass microwave signal based on the photonic microwave bandpass differentiator. (a) Waveform of the microwave baseband signal. (b) Experimental differentiation result of the input signal shown in (a). (c) Ideal differentiation result of the input signal shown in (a)

5.4 Discussion and conclusion

For the experimented differentiator, the power penalty function due to the chromatic dispersion of the SMF has a 3-dB bandwidth of 13.72 GHz, which is greater than 9.95 GHz. Therefore, power fading due the chromatic dispersion of the fiber is small and can be ignored. However, for the same chromatic dispersion, if the differentiator is designed to operate at a much higher frequency, for example, if the 4^{th} channel of the spectral response is used to perform the differentiation, the center frequency is 39.8 GHz, then the power fading effect must be taken into consideration. A simple solution

to this problem is to use SSB modulation scheme [74] instead of the double-side band (DSB) modulation scheme employed here.

In summary, a microwave bandpass differentiator implemented based on a FIR photonic microwave delay-line filter with nonuniformly-spaced taps was proposed and experimentally demonstrated. The key contribution of this work is that a differentiator was designed and demonstrated using a photonic microwave delay-line filter with all positive coefficients, which greatly simplified the implementation. The negative coefficients were equivalently achieved by introducing additional time delays, leading to a π phase shift to each of the negative taps. A microwave bandpass differentiator based on a six-tap FIR microwave photonic delay-line filter was designed, simulated and experimentally demonstrated. The reconfigurability of the differentiator was experimentally investigated. The differentiation of a bandpass microwave signal using the six-tap differentiator was also experimentally demonstrated.

Other than the photonic microwave bandpass differentiator, many photonic microwave signal processors can be implemented using non-uniformly spaced photonic microwave filter. For example, a photonic microwave bandpass Hilbert transformer can be achieved by carefully designed the tap coefficients.

CHAPTER 6 CONCLUSION AND FUTURE WORK

6.1 Conclusion

All optical processing of microwave signals was investigated in this thesis. Two techniques were developed. At first, implementation of a photonic-assisted microwave pulse fractional Hilbert transformer with tunable fractional order based on TPS was proposed and experimentally demonstrated. The fractional Hilbert transform was realized by introducing a phase jump to the spectrum of the input pulse via phase modulation and the tunability of the fractional order was achieved by changing the amplitude of the step function applied to the PM. The key advantage of this technique is its flexibility in changing the fractional order, which may find applications where a Hilbert transform with a tunable order is needed.

Second, a microwave bandpass differentiator implemented based on a FIR photonic microwave delay-line filter with nonuniformly-spaced taps was proposed and experimentally demonstrated. The key contribution of this work is that a differentiator was designed and demonstrated using a photonic microwave delay-line filter with all positive coefficients, which greatly simplified the implementation. The negative coefficients were equivalently achieved by introducing additional time delays, leading to a π phase shift to each of the negative taps. A microwave bandpass differentiator based on a six-tap FIR microwave photonic delay-line filter was designed, simulated and experimentally demonstrated. The reconfigurability of the differentiator was

experimentally investigated. The differentiation of a bandpass microwave signal using the six-tap differentiator was also experimentally demonstrated.

6.2 Future work

Temporal pulse shaping has been widely investigated in the past few years due to its important applications in the areas such as frequency analysis [26] and arbitrary waveform generation [27]-[30]. In Chapter 4, the implementation of a photonic-assisted microwave pulse fractional Hilbert transformer with tunable fractional order based on TPS was proposed and experimentally demonstrated. The spectrum of the input pulse can be directly filtered in the temporal domain via the electrical arbitrary waveform generator and the electro-optic modulator. In the experiment for demonstration, since the output signal of the Hilbert transformer is an ultra high speed optical pulse, it cannot be directly detected by the PD. To monitor the output pulse, another 6.74-km SMF (SMF2) with a value of dispersion of -890 ps^2 was used to stretch the output pulse, to make it wide enough to be detected by the PD. The experimental result is confirmed with the simulated result. The experimental results may need to be further confirmed using other method such as employing an autocorrelator to detect the ultra short pulse [75].

In Chapter 5, a photonic microwave bandpass differentiator was proposed and experimentally demonstrated. Other than the photonic microwave bandpass differentiator, many photonic microwave signal processors can be implemented using

a nonuniformly spaced photonic microwave filter. For example, a photonic microwave bandpass Hilbert transformer can be achieved by carefully designing the tap coefficients. Based on a nonuniformly-spaced photonic microwave filter, many signal processing functions can be implemented. The performance of other signal processors based on nonuniformly-spaced can be investigated in the future.

For the experimented differentiator, a photonic microwave bandpass differentiator with a relative bandwidth of 0.2 is designed. Based on our experimental conditions, a differentiator with a center frequency of 9.95 GHz and a bandwidth of 2 GHz was realized. A larger bandwidth passband can be achieved when a higher center frequency is used. The performance of the microwave photonic differentiator with a higher center frequency and larger bandwidth will be investigated.

In this thesis, the implementation of a Hilbert transformer and a differentiator was experimentally demonstrated. The experimental systems were realized using discrete optical devices, such as lasers, electro-optic modulator, optical couplers and PDs. The systems were bulky and costly, which limits the potential for practical applications. A promising solution to this problem is to use photonic integrated circuits (PICs). It was demonstrated recently [76], a PIC consisting of a hybrid laser source, a modulator and passive components can be integrated into a single chip. The integration technology can be employed to implement the proposed signal processing systems, to increase the system performance.

REFERENCE

[1] A. J. Seeds and K. J. Williams, "Microwave Photonics," *J. Lightw. Technol.*, vol. 24, no .12, pp. 4628-4641, Dec. 2006.

[2] J. P. Yao, "Microwave photonics," *J. Lightw. Technol.*, vol. 27, no. 3, pp. 314-335, Feb. 2009.

[3] J. Capmany and D. Novak, "Microwave photonics combines two worlds," *Nature Photon.*, vol. 1, no. 6, pp. 319–330, Jun. 2007.

[4] J. Capmany, B. Ortega, D. Pastor, and S. Sales, "Discrete-time optical processing of microwave signals," *J. Lightw. Technol*., vol. 23, no. 2, pp. 702-723, Feb. 2005.

[5] R. A. Minasian, "Photonic signal processing of microwave signals," *IEEE Trans. Microw. Theory Tech*., vol. 54, no. 2, pp. 832- 846, Feb. 2006.

[6] K. Jackson, S. Newton, B. Moslehi, M. Tur, C. Cutler, J. Goodman, and H. J. Shaw, "Optical fiber delay-line signal processing," *IEEE Microw. Theory Tech.*, vol. 33, no. 3, pp. 193–204, Mar. 1985.

[7] Y. Han, Z. Li, S. Pan, M. Li, and J. P. Yao, "Photonic-assisted tunable microwave pulse fractional Hilbert transformer based on a temporal pulse shaping system," *IEEE Photon. Technol. Lett.*, vol. 23, no. 9, pp. 570-572, May 2011.

[8] J. P. Yao, Photonic generation of microwave arbitrary waveforms, *Opt. Comm.*, vol. 284, no. 15, pp. 3723-3736, Jul. 2011.

[9] J. P. Heritage, and A. M. Weiner, "Optical systems and methods based upon temporal stretching, modulation and recompression of ultrashort pulses," U. S. Patent 4 928 316, May 22, 1990.

[10] A. M. Weiner, “Femtosecond pulse shaping using spatial light modulators,” *Rev. Sci. Instrum.* , vol. 71, no. 5, pp. 1929–1960, May 2000.

[11] D. E. Leaird, and A. M. Weiner, “Femtosecond direct space-to-time pulse shaping,” *IEEE Quantum Electron.*, vol. 37, no. 4, pp. 494-504, Apr. 2001.

[12] D. E. Leaird, and A. M. Weiner, “Femtosecond direct space-to-time pulse shaping in an integrated-optic configuration,” *Opt. Lett*., vol. 29, no. 13, pp. 1551-1553, Jul. 2004.

[13] A. M. Weiner, J. P. Heritage, and E. M. Kirschner, “High-resolution femtosecond pulse shaping," *J. Opt. Soc. Am. B.*, vol. 5, no. 8, pp. 1563-1572, Aug. 1988.

[14] A. M. Weiner, D. E. Leaird, J. S. Patel, and J. R. Wullert, “Programmable femtosecond pulse shaping by use of a multielement liquid-crystal phase modulator,” *Opt. Lett.* vol. 15, no. 6, pp. 326-328, Mar. 1990.

[15] M. A. Dugan, J. X. Tull, and W. S. Warren, “High-resolution acousto-optic shaping of unamplified and amplified femtosecond laser pulses,” *J. Opt. Soc. Am. B.*, vol. 14, no. 9, pp. 2348-2358, Sep. 1997.

[16] J. D. Mckinney, D. E. Leaird, and A. M. Weiner, “Millimeter-wave arbitrary waveform generation with a direct space-to-time pulse shaper,” *Opt. Lett.*, vol. 27, no, 15, pp. 1345-1347, Aug. 2002.

[17] C. Wang, F. Zeng, and J. P. Yao, “All-Fiber Ultrawideband pulse generation based on spectral shaping and dispersion-induced frequency-to-time conversion,” *IEEE Photon. Technol. Lett.* , vol. 19, no. 3, pp. 137-139, Feb. 2007.

[18] H. Chi, F. Zeng, and J. P. Yao, “Photonic generation of microwave signals based on pulse shaping,” *IEEE Photon. Technol. Lett.*, vol. 19, no. 9, pp. 668-670, May 2007.

[19] H. Chi and J. P. Yao, “All-fiber chirped microwave pulse generation based on spectral shaping and wavelength-to-time conversion,” *IEEE Trans. Microw. Theory Tech.*, vol. 55, no. 9, pp. 1958-1963, Sep. 2007.

[20] C. Wang and J. P. Yao, “Photonic generation of chirped millimeter-wave pulses based on nonlinear frequency-to-time mapping in a nonlinearly chirped fiber Bragg grating,” *IEEE Trans. Microwav. Theory Tech.*, vol. 56, no. 2, pp. 542-553, Feb. 2008.

[21] H. Chi and J. P. Yao, “Chirped RF pulse generation based on optical spectral shaping and wavelength-to-time mapping using a nonlinearly chirped fiber Bragg grating,” *J. Lightw. Technol.*, vol. 26, no. 10, pp. 1282-1287, May 2008.

[22] C. Wang and J. P. Yao, “Photonic generation of chirped microwave pulses using superimposed chirped fiber Bragg gratings,” *IEEE Photon. Technol. Lett.*, vol. 20, no. 11, pp. 882-884, Jun. 2008.

[23] C. Wang and J. P. Yao, “Simultaneous optical spectral shaping and wavelength-to-time mapping for photonic microwave arbitrary waveform generation,” *IEEE Photon. Technol. Lett.*, vol. 21, no. 12, pp. 793-795, Jun. 2009.

[24] T. Jannson, “Real-Time Fourier Transformation in Dispersive Optical Fibers,” *Opt. Lett*., vol. 8, no. 4, pp. 232-234, Apr. 1983.

[25] M. A. Muriel, J. Azana, and A. Carballar, “Real-time Fourier transformer based fiber grating,” *Opt. Lett.*, vol. 24, no. 1, pp. 1–3, Jan. 1999.

[26] R. E. Saperstein, D. Panasenko, and Y. Fainman, “Demonstration of a microwave spectrum analyzer based on time-domain optical processing in fiber,” *Opt. Lett.* vol. 29, no. 5, pp. 501-503, Mar. 2004.

[27] H. Chi and J. P. Yao, “Symmetrical waveform generation based on temporal pulse shaping using an amplitude-only modulator,” *Electron. Lett.*, vol. 43, no. 7, pp. 415-417, Mar. 2007.

[28] S. Thomas, A. Malacarne, F. Fresi, L. Potì, and J. Azaña, “Fiber-Based Programmable Picosecond Optical Pulse Shaper,” *J. Lightw. Technol.*, vol. 28, pp. 1832-1843, Feb. 2010.

[29] J. Azana, N. K. Berger, B. Levit, and B. Fischer, “Reconfigurable generation of high-repetition-rate optical pulse sequences based on time domain phase-only filtering,” *Opt. Lett.*, vol. 30, no. 23, pp. 3228-3230, Dec. 2005.

[30] M. Li, C. Wang, W. Li, and J. P. Yao, “An unbalanced temporal pulse shaping system for chirped microwave waveform generation,” *IEEE Trans. Microw. Theory Tech.*, vol. 58, no. 11, pp. 2968-2975, Nov. 2010.

[31] T. X. H. Huang, X. Yi, and R. A. Minasian, “Single passband microwave photonic filter using continuous-time impulse response,” *Opt. Express*, vol. 19, no. 7, pp. 6231-6242, Mar. 2011.

[32] S. Xiao, A. M. Weiner, “Coherent Photonic Processing of Microwave Signals Using Spatial Light Modulators: Programmable Amplitude Filters,” *J. Lightw. Technol.*, vol. 24, no. 7, Jul. 2006.

[33] S. Xiao, A. M. Weiner, “Programmable Photonic Microwave Filters With Arbitrary Ultra-Wideband Phase Response,” *IEEE Trans. Microw. Theory Tech.*, vol. 54, no. 11, pp. 4002-4008, Nov. 2006.

[34] E. Hamidi, and A. M. Weiner, “Phase-Only Matched Filtering of Ultrawideband Arbitrary Microwave Waveforms via Optical Pulse Shaping,” *J. Lightw. Technol.*, vol. 26, no. 15, pp. 2355-2363, Aug. 2008.

[35] T. Mengual, B. Vidal, and J. Marti, “Photonic microwave filter based on a spatial light modulator with continuous tuning capability,” *2008 International Topical Meeting on Microwave Photonics.*, pp.106-109, Oct. 2008.

[36] R. Slavík, Y. Park, M. Kulishov, R. Morandotti, and J. Azaña, “Ultrafast all-optical differentiators,” *Opt. Express*, vol.14 no. 22, pp. 10699-10707, Oct. 2006.

[37] N. K. Berger, B. Levit, B. Fischer, M. Kulishov, D. V. Plant, and J. Azaña, “Temporal differentiation of optical signals using a phase-shifted fiber Bragg grating,” *Opt. Express*, vol. 15, no. 2, pp. 371–381, Jan. 2007.

[38] M. Kulishov, and J. Azaña, “Long-period fiber gratings as ultrafast optical differentiators,” *Opt. Lett.*, vol. 30, no. 20, pp. 2700–2702, Oct. 2005.

[39] M. Li, D. Janner, J. P. Yao, and V. Pruneri, “Arbitrary-order all-fiber temporal differentiator based on a fiber Bragg grating: design and experimental demonstration,” *Opt. Express*, vol. 17, no. 22, pp. 19798-19807, Oct. 2009.

[40] M. H. Asghari and J. Azaña, “On the Design of Efficient and Accurate Arbitrary-Order Temporal Optical Integrators Using Fiber Bragg Gratings,” *J. Lightw. Technol.*, vol. 27, no. 17, pp. 3888-3895, Sep. 2009.

[41] M. H. Asghari and J. Azaña, “All-optical Hilbert transformer based on a single phase-shifted fiber Bragg grating: design and analysis,” *Opt. Lett.* vol. 34, no. 3, pp. 334-336, Feb. 2009.

[42] M. Li and J. P. Yao, “All-fiber temporal photonic fractional Hilbert transformer based on a directly designed fiber Bragg grating,” *Opt. Lett.*, vol. 35, no. 2, pp. 223-225, Jan. 2010.

[43] C. Wang, M. Li, and J. P. Yao, "Continuously tunable photonic microwave frequency multiplication by use of an unbalanced temporal pulse shaping system," *IEEE Photon. Technol. Lett.*, vol. 22, no. 17, pp. 1285-1287, Aug. 2010.

[44] K. Wilner and A. P. Va den Heuvel, “Fiber-optic delay lines for microwave signal processing,” *Proc. IEEE*, vol. 64, no. 5, pp. 805–807, May 1976.

[45] C. Chang, J. A. Cassaboom, and H. F. Taylor, “Fiber optical delay line devices for RF signal processing,” *IEE Electron. Lett*., vol. 13, no. 22, pp. 678–680, Oct. 1977.

[46] J. Capmany, J. Cascon, J.L. Martin, S. Sales, D. Pastor, and J. Marti, “Synthesis of fiber-optic delay line filters,” *J. Lightw. Technol.*, vol.13, no.10, pp. 2003-2012, Oct. 1995.

[47] X. Wang and K. T. Chan, “Tunable all-optical incoherent bipolar delay-line filter using injection-locked Fabry-Perot laser and fiber Bragg gratings,” *Electron. Lett*., vol. 36, no. 24, pp. 2001–2002, Nov. 2000.

[48] S. Li, K. S. Chiang, W. A. Gambling, Y. Liu, L. Zhang, and I. Bennion, “A novel tunable all-optical incoherent negative-tap fiber-optical transversal filter based on a DFB laser diode and fiber Bragg gratings,” *IEEE Photon. Technol. Lett*., vol. 12, no. 9, pp. 1207–1209, Sep. 2000.

[49] J. Mora, M. V. Andres, J. L. Cruz, B. Ortega, J. Capmany, D. Pastor, and S. Sales, “Tunable all-optical negative multitap microwave filters based on uniform fiber Bragg gratings,” *Opt. Lett*., vol. 28, no. 15, pp. 1308–1310, Aug. 2003.

[50] B. Vidal, J. L. Corral, and J. Marti, “All-optical WDM multi-tap microwave filter with flat bandpass,” *Opt. Express*, vol. 14, no. 2, pp. 581–586, Jan. 2006.

[51] J. Wang, F. Zeng, and J. P. Yao, “All-optical microwave bandpass filter with negative coefficients based on PM-IM conversion,” *IEEE Photon. Technol. Lett*., vol. 17, no. 10, pp. 2176–2178, Oct. 2005.

[52] J. P. Yao and Q. Wang, “Photonic microwave bandpass filter with negative coefficients using a polarization modulator,” *IEEE Photon. Technol. Lett*., vol. 19, no. 9, pp. 644–646, May 2007.

[53] Q. Wang and J. P. Yao, “Multi-tap photonic microwave filters with arbitrary positive and negative coefficients using a polarization modulator and an optical polarizer,” *IEEE Photon. Technol. Lett*., vol. 20, no. 2, pp. 78–80, Jan. 2008.

[54] F. Coppinger, S. Yegnanarayanan, P. D. Trinh, and B. Jalali, “All-optical RF filter using amplitude inversion in a semiconductor optical amplifier,” *IEEE Trans. Microw. Theory Tech.*, vol. 45, no. 8, pp. 1473-1477, Aug. 1997.

[55] Y. Yan, F. Zeng, Q. Wang, and J. P. Yao, “Photonic microwave filter with negative coefficients based on cross polarization modulation in a semiconductor optical amplifier,” in OFC 2007, 2007, Paper OWU6.

[56] J. Capmany, D. Pastor, A. Martinez, B. Ortega, and S. Sales, “Microwave photonic filters with negative coefficients based on phase inversion in an electro-optic modulator,” *Opt. Lett*., vol. 28, no. 16, pp. 1415-1417, Aug. 2003.

[57] F. Zeng, J. Wang, and J. P. Yao, “All-optical microwave bandpass filter with negative coefficients based on a phase modulator and linearly chirped fiber Bragg gratings,” *Opt. Lett*., vol. 30, no.17, pp. 2203-2205, Sep. 2005.

[58] A. Loayssa, J. Capmany, M. Sagues, and J. Mora, “Demonstration of incoherent microwave photonic filters with all-optical complex coefficients,” *IEEE Photon. Technol. Lett*., vol. 18, no. 16, pp. 1744-1746, Aug. 2006.

[59] Y. Yan and J. P. Yao, “A tunable photonic microwave filter with complex coefficient using an optical RF phase shifter,” *IEEE Photon. Technol. Lett*., vol. 19, no. 19, pp. 1472-1474, Oct. 2007.

[60] Y. Dai and J. P. Yao, “Nonuniformly-spaced photonic microwave delay-line filter,” *Opt. Express*, vol. 16, no. 7, pp. 4713-4718, Mar. 2008.

[61] Y. Dai and J. P. Yao, “Nonuniformly spaced photonic microwave delay-line filters and applications,” *IEEE Trans. Microw. Theory Tech.*, vol. 58, no. 11, pp. 3279-3289, Nov. 2010.

[62] V. Torres-Company, J. Lancis, and P. Andrés, “Incoherent frequency-to-time mapping: application to incoherent pulse shaping,” *J. Opt. Soc. Am. A*, vol. 24, no. 3, pp. 888-894, Mar. 2007.

[63] C. Dorrer, “Statistical analysis of incoherent pulse shaping,” *Opt. Express*, vol. 17, no. 5, pp. 3341-3352, Mar. 2009.

[64] Y. Park and J. Azaña, “Optical signal processors based on a time-spectrum convolution,” *Opt. Lett.*, vol. 35, no. 6, pp. 796-798, Mar. 2010.

[65] Y. Park and J. Azaña, “Ultrahigh dispersion of broadband microwave signals by incoherent photonic processing,” *Opt. Express*, vol. 18, no. 14, pp. 14752-14761, Jul. 2010.

[66] S. L. Hahn, “Hilbert Transforms,” in *The Transforms and Applications Handbook*, A. D. Poularikas, Ed., 3rd ed., Ch. 7, CRC, 2009.

[67] A. W. Lohmann, D. Mendlovic, and Z. Zalevsky, “Fractional Hilbert transform,” *Opt. Lett.*, vol. 21, no. 4, pp.281-283, Feb. 1996.

[68] F. Zeng and J. P. Yao, “Ultrawideband impulse radio signal generation using a high-speed electrooptic phase modulator and a fiber-Bragg-grating-based

frequency discriminator," *IEEE Photon. Technol. Lett.*, vol. 18, no. 19, pp. 2062-2064, Oct. 2006.

[69] J. Xu, X. Zhang, J. Dong, D. Liu, and D. Huang, "High-speed all-optical differentiator based on a semiconductor optical amplifier and an optical filter," *Opt. Lett*., vol. 32, no. 13, pp. 1872-1874, Jul. 2007.

[70] J. Xu, X. Zhang, J. Dong, D. Liu, and D. Huang, "All-optical differentiator based on cross-gain modulation in semiconductor optical amplifier," *Opt. Lett*., vol. 32, no. 20, pp. 3029-3031, Oct. 2007.

[71] Z. Li and C. Wu, "All-optical differentiator and high-speed pulse generation based on cross-polarization modulation in a semiconductor optical amplifier," *Opt. Lett*., vol. 34, no. 6, pp. 830-832, Mar. 2009.

[72] J. G. Proakis and D. G. Manolakis, "Design of digital filters," in *Digital Signal Processing*, 4th ed., Ch. 10, Prentice Hall, 2009.

[73] J. P. Yao, F. Zeng, and Q. Wang, "Photonic generation of Ultra-Wideband signals," *J. Lightw. Technol.*, vol. 25, no. 11, pp. 3219-3235, Nov. 2007.

[74] G. H. Smith, D. Novak, and Z. Ahmed, "Overcoming chromatic-dispersion effects in fiber-wireless systems incorporating external modulators," *IEEE Trans. Microw. Theory Tech*., vol. 45, no. 8, pp. 1410-1415, Aug. 1997.

[75] M. Li, Y. Han, S. Pan, and J. P. Yao, "Experimental demonstration of symmetrical waveform generation based on amplitude-only modulation in a temporal pulse shaping system," *IEEE Photon. Technol. Lett*., vol. 23, no. 11, pp. 715-717, Jun. 2011.

[76] B. R. Koch, A. Alduino, L. Liao, R. Jones, M. Morse, B. Kim, W. Lo, J. Basak, H. Liu, H. Rong, M. Sysak, C. Krause, R. Saba, D. Lazar, L. Horwitz, R. Bar, S. Litski, A. Liu, K. Sullivan, O. Dosunmu, N. Na, T. Yin, F. Haubensack, I. Hsieh, J. Heck, R. Beatty, J. Bovington, and M. J. Paniccia, “A 4x12.5 Gbps CWDM Si Photonics Link using Integrated Hybrid Silicon Lasers,” in CLEO 2011, 2011, Paper CThP5.

LIST OF ACRONYMS

A

AWG	Arbitrary waveform generation
ASE	Amplified spontaneous emission

D

DE	Dispersive element
DLP	Discrete layer peeling
DSB	Double-side band
DSB-SC	Double-sideband suppressed-carrier
DST	Direct space to time

E

E/O	Electrical-to-optical conversion
EOM	Electro-optic modulator

F

FBG	Fiber Bragg grating
FIR	Finite impulse response
FSR	Free spectral range
FT	Fourier transform
FWHM	Full-width at half-maximum

G

GVD	Group velocity dispersion

I

IM	Intensity modulator

L

LC-FBG	Linearly-chirped FBG
LC-SLM	Liquid crystal SLM
LTI	Linear, time-invariant

M

MLL	Mode-locked laser
MZM	Mach-Zehnder modulator

N

NRMSE	Normalized root mean square error

O

O/E	Electrical-to-optical conversion

P

PC	Polarization controller
PD	Photodetector
PS-FBG	Phase shift fiber Bragg grating
PIC	Photonic integrated circuit
PM	Phase modulator
PM-IM	Phase-modulation to intensity-modulation

R

RF	Radio frequency

S

SBS	Stimulated Brillouin scattering
SLM	Spatial light modulator
SNR	Signal-to-noise ratio
SOA	Semiconductor optical amplifier
SSB	Single-sideband modulation

T

TOD	Third order dispersion
TPS	Temporal pulse shaping

U

UWB	Ultra wide band

X

XGM	Cross-gain modulation
XPolM	Cross-polarization modulation

LIST OF PUBLICATIONS

[1] Y. Han, Z. Li, S. Pan, M. Li, and J. P. Yao, “Photonic-assisted tunable microwave pulse fractional Hilbert transformer based on a temporal pulse shaping system,” *IEEE Photon. Technol. Lett.*, vol. 23, no. 9, pp. 570-572, May 2011.

[2] Y. Han, Z. Li, and J. P. Yao, “A Microwave Bandpass Differentiator Implemented Based on a Nonuniformly-Spaced Photonic Microwave Delay-Line Filter,” *J. Lightw. Technol.*, submitted.

[3] M. Li, Y. Han, S. Pan, and J. P. Yao, “Experimental demonstration of symmetrical waveform generation based on amplitude-only modulation in a temporal pulse shaping system,” *IEEE Photon. Technol. Lett.*, vol. 23, no. 11, pp. 715-717, Jun. 2011.